ICARUS 108, 37–58 (1994)

Is There a Planet around β Pictoris? Perturbations of a Planet on a Circumstellar Dust Disk

1. The Numerical Model

FRANÇOISE ROQUES

Observatoire de Paris, DAEC/EUROPA, 92195 Meudon Cédex, France
E-mail: roques@mesioa.obspm.circe.fr

HANS SCHOLL

Observatoire de Nice, Dept. Cassini, B.P. 229, 06304 Nice Cédex 4, France

BRUNO SICARDY

Université Pierre et Marie Curie, 75005 Paris Cédex, France, and Observatoire de Paris, DAEC/EUROPA, 92195 Meudon Cédex, France

AND

BRADFORD A. SMITH

University of Hawaii, Institute for Astronomy, Honolulu, Hawaii 96822

Received July 6, 1993; revised January 10, 1994

The β Pictoris circumstellar disk, like others, seems to exhibit an inner clearing zone, at typical distances of 1–50 AU from the star. We investigate the possibility that this void is caused by a planet embedded in the disk. We have implemented on a Connection Machine a code which simultaneously integrates the motions of 8192 particles. These are submitted to Poynting–Robertson (PR) drag, while being perturbed by a planet orbiting at 20 AU from the star. The free parameters are the planetary mass, the planetary orbital eccentricity, and the particle size. Above a critical planet mass of $\sim 10^{-5}$ stellar masses (~5 Earth masses, or $\frac{1}{3}$ Uranian masses), the planet is able to trap particles in outer mean motion resonances, for time scales comparable to, or larger than, the PR decay time. No permament trapping is observed, however. Once they escape the resonances, the particles rapidly decay onto the star, on highly eccentric orbits. A moderate planetary orbital eccentricity (10^{-2}) can create large arclike structures in the disk. A depleted region corotating with the planet, and just outside it, is also observed. We show finally that these processes can create a steady state clearing zone extending inside the planet orbit. We emphasize that the structures excited on the disk by a planet could be a way to reveal bodies otherwise invisible by direct imagery.

1. INTRODUCTION

Due to the increasing quality of observations, circumstellar regions have recently excited a growing interest, in particular because they may be the cocoons from which planets form. They are thus fundamental clues to understanding the formation and the evolution of planetary systems, including ours. IRAS data imply that most of the A, F, and G stars have dusty disks (Aumann, 1988). Also, between 25 and 50% of pre-main-sequence stars and T Tauri stars have detectable circumstellar disks (see the reviews by Beckwith *et al.* 1990, Beckwith and Sargent 1993, and Basri and Bertout 1993). Until recently, only the disk surrounding the nearby star β Pictoris has been directly detected by imagery (Smith and Terrile 1984, 1987, Paresce and Burrows 1987, Vidal-Madjar *et al.* 1992, Lecavelier des Etangs *et al.* 1993, and see the review by Norman and Paresce 1989).

Many other stars are strongly suspected to be surrounded by disks, such as α Piscis Austrini (Fomalhaut), α Lyrae (Vega), τ_1 Eridani, ε Eridani (Chini *et al.* 1990, Chini *et al.* 1991, Stern *et al.* 1993), ε Aurigae (Ferluga 1990), and HD 98800 (Zuckerman and Becklin 1993), among others.

In the case of β Pictoris, the comparison of visible images with infrared observations indicates that there is an inner clearing zone at typical planetary distances (a few to ~30 AU according to the models) from the star; see Section 2. Similar conclusions are reached about Fomalhaut, Vega, τ_1-Eridani, ε-Eridani, with inner bound-

0019-1035/94 $6.00

aries for the disk ranging from ~10 to 50 AU, according to the star (Chini *et al.* 1991). These depleted zones raise dynamical problems, since the dust particles are subjected to various drags, and should fall rapidly onto the star, thus filling in the inner zone.

Several hypotheses can be proposed, and are discussed in Section 2. We retain in this paper one of them, namely that a planet revolves in the disk and confines its inner edge. The physics at work is more precisely the interplay between mean motion resonances with the planet and Poynting–Robertson (PR) drag acting on the grains. The complete physics involved in the birth and evolution of these disks is certainly very complex (gas drag, collisions, gravitational scattering by planetesimals, etc.). For a better understanding of this system, however, we would like to *isolate* one process only. Although we use the parameters relevant to the β Pictoris system, our study is easily applicable to other circumstellar disks. The points that we address here are thus the following:

- Is a planet able to confine an inner edge of the disk, and what is the minimum mass for this to be possible? Although other explanations may be proposed, this one could be valid for some circumstellar disks.
- Are other structures created by the planet? Are such structures, like gaps, large enough to be imaged in the near future (see the discussion by Paresce 1992)? So, even though the planet is not detectable directly, its effects on the disk could be visible from the Earth. As we shall see, the features driven by the alleged planet (arc-like structures or void following the planet) could discriminate among various hypotheses, such as sublimation effects, enhanced gas drag near the star, or perturbations by a hypothetical brown dwarf (see Whitmire *et al.* 1989).
- As we discuss in the next section, a planet could also be the cause for the infalling of comet-like bodies onto the star. Within this perspective, it is important to have a consistent model in which a planet can, at the same time, shape the circumstellar disk, throw comet-like objects onto the star or eject them to the outer boundaries of the disk, stir the disk to increase its thickness, etc. Again, our model is not intended to be universal, but rather, a first step for better understanding circumstellar disks perturbed by planets.
- From a broader point of view, the effect of a planet on a dust disk may have important implications for the confinement of material in the disk, and thus can be an important step for the accretion of new bodies.

In this paper, we study numerically the perturbations that a planet induces on a disk composed of test particles. The code is implemented on a Connection Machine, a massively parallel computer (Scholl *et al.* 1993). It enables us to simulate the evolution of 8192 test particles at a time. This large number can reveal collective patterns excited by the planet (Roques *et al.* 1990), much more easily than the tedious accumulation of isolated runs with one particle only. This study can be seen as an experiment, which requires more theoretical work once dynamical processes have been more clearly identified. In a companion paper (Lazzaro *et al.* 1994, hereafter referred to as Paper 2), we analyze the mechanism of capture itself into first order resonances in more detail. Our aim in this second paper is to give analytical support to the mechanisms revealed in the present paper.

We first briefly review in Section 2 the main characteristics of the β Pictoris system. The various forces acting on a dust particle are discussed in Section 3. The numerical model is described in Section 4. The results are presented in Section 5, with a discussion of the sensitivity to the various parameters (planet mass, orbital eccentricity, particle size, disk thickness, etc.) A discussion is given in the final section.

2. THE β PICTORIS DISK: PHYSICAL PROPERTIES

The β Pictoris star is believed to be a young A5 dwarf with an age less than $\sim 2 \times 10^8$ years, located at 17 parsecs from the Earth, with a mass of 1.5 $M_\odot$ and a luminosity of 6 $L_\odot$ (Norman and Paresce 1989, Paresce 1991). The coronographic images show a nearly edge-on disk with an extension of more than 1000 AU (Smith and Terrile 1987), and an opening angle of 8° (Artymowicz *et al.* 1989). The images reveal furthermore as asymmetry in the structure of the two ansae of the disk at large distances, the northeast projection extending to more than 1100 AU, and the southwest projection extending to only ~900 AU (Smith and Terrile 1987). The inner part of the disk also exhibits an asymmetry in brightness, but reversed with respect to the outer regions (Vidal-Madjar *et al.* 1992, Lecavelier des Etangs *et al.* 1993). These latter observations show that the particle albedo is neutral in B, V, R, and Ic at distances larger than 75 AU, and that the albedo drops by a factor of 4 from 75 to 30 AU in the B band. This reddening could be explained by particles becoming more dusty (less icy) when going inward. Independent observations of the β Pictoris system confirm the evidence of changing disk structure within 100 AU (Golimowski *et al.* 1993, Lagage and Pantin 1993).

Coronographic images taken in the visible and IRAS data and ground-based IR observations can be combined to constrain the radial distribution of the dust around the star, together with the size distribution of the grains. Several models have been developed; there is no unique solution, but some general structural features of the disk have been recognized. A model by Artymowicz *et al.* (1989) gives grain radii in the range 1–20 μm, with a high albedo >0.5. The minimum grain radius of 1 μm is confirmed by independent observations (Norman and Paresce 1989). The combination of IRAS and corono-

graphic data requires that the inner part of the disk is largely cleared. However, while the existence of this clearing zone seems to be well established, its size is very model dependent, with a radius varying between 5 and 36 AU for μm-sized particles (Artymowicz *et al.* 1989, Chini *et al.* 1990, and Chini *et al.* 1991). According to these authors, the optical depth could be as large as 7×10^{-3} at the densest part of the disk. The estimated total mass of the dust disk is one lunar mass.

Some alternative models have been proposed more recently by Backman *et al.* 1992), using visible data and IRAS fluxes, plus IR ground-based observations (10 and 20 μm). In order to fit all these observations, this model requires a two-component disk. An outer ($r > 80$ AU) disk would be made of icy particles, and an inner ($r < 80$ AU) disk would be made of refractory material, with a significant deficit of material with respect to an inward extrapolation of the outer component. This inner disk either would be made of smaller particles, compared to the outer disk, or would have a flatter radial density distribution than the outer disk. The minimum grain size would be in the range ~0.4–3 μm, assuming a power law with an index of -3.5 for the differential size distribution of the grains (number of particles with radii between s and $s + ds$ proportional to $s^{-3.5}$). The normal optical depth of their preferred model is $\sim 5 \times 10^{-4}$, around 20 AU. Finally, the inner disk should also have an inner limit between 1 and 30 AU, defining an innermost void.

Alternative models includes millimeter data as well as optical and IR data. These models indicate that large particles should be present, at least 5 mm in radius and possibly more (Chini *et al.*, 1991). This model requires an inner cavity of ~35 AU, and a disk mass of ~0.5 Earth masses (~40 lunar masses). Similar conclusions are reached by Zuckerman and Becklin (1993) concerning Vega, Fomalhaut, and β Pictoris, with disk masses ranging from 0.1 to 10 lunar masses, contained in millimeter-sized particles.

UV spectroscopic observations of β Pictoris show transient red-shifted absorption lines corresponding to material falling onto the star. These observations are highly variable, with time scales ranging from some hours to some months (Norman and Paresce 1989, Beust *et al.* 1990, 1991, Beust 1991, Boggess *et al.* 1991, Beust and Tagger 1993). This material could originate from the sublimation of comets perturbed by a planet and vaporized as they fall onto the star.

In a protoplanetary disk, the dust is either primordial (nebula condensates) or produced by cometary activity and collisions between larger planetesimals. The age of β Pictoris and the tenuous density of the gas argue in favor of the second mechanism. In this case, the disk corresponds to a short period of protoplanetary evolution, after the gas shell has been ejected, when the planetesimals are still accreting into a few large bodies. The opening angle of the dust distribution also argues in favor of large bodies stirring the disk and providing the dust through collisions. On the other hand, theoretical models yield some constraints on the size distribution of the solid material in a protoplanetary nebula: the gaseous component causes a very rapid inward drift of the grains. So, unless the dust is confined in a very thin subdisk, in which the gas drag should be reduced, the accretion of kilometer-sized bodies must occur before the ejection of the gas (see the reviews by Lissauer 1987, 1993). So the 3D structure of the β Pictoris disk implies that the gas ejection happened when a large part of the solid material was already in the form of kilometer-sized bodies.

3. FORCES ACTING ON A GRAIN

A complete review of the forces acting on a circumstellar dust grain is done in the case of the solar system by Leinert and Grün (1990). The variables used here are defined in the Appendix of Paper 2.

3.1. Nongravitational Forces and Processes

Radiation forces are due to the absorption and re-emission, by a particle, of the momentum carried by the stellar photons. The reader is referred to the papers by Burns *et al.* (1979) and by Leinert and Grün (1990) for a thorough discussion of these forces. The corresponding acceleration is

$$\gamma_R = \left(\frac{GM_\star\beta}{r^2}\right)\left[\left(1 - \frac{\dot{r}}{c}\right)\mathbf{u}_r - \frac{\mathbf{v}}{c}\right], \qquad (1)$$

where G is the constant of gravitation, $M_\star$ is the mass of the star, r is the distance to the star, c is the velocity of light, $\dot{r}$ and $\mathbf{v}$ are the radial and total velocity of the grain, and $\mathbf{u}_r$ is the unit vector in the direction of the incident radiation. The constant term in (1) is referred to as the *pressure of radiation,* while the velocity-dependent term is referred to as the *Poynting–Robertson* (PR) drag. Finally, β is by definition the (constant) ratio of the radiation pressure to the gravitational attraction of the star. Its value depends on the particle size and on its optical properties, as discussed below.

The pressure of radiation being opposed and proportional to the gravitational pull of the star, its effect is strictly equivalent to changing the mass of the latter by a factor of $1 - \beta$. This changes the mean motion and orbital velocity of the particle, with respect to their local Keplerian mean values, by a factor $\sqrt{1 - \beta}$. This effect changes the location of the mean motions resonances, as seen later. The PR drag causes decay of the particle semimajor axis a and orbital eccentricity e, at the rates (Burns *et al.* 1979)

$$\dot{a} = -\alpha a \frac{2 + 3e^2}{(1 - e^2)^{3/2}} \tag{2}$$

$$\dot{e} = -\alpha \frac{5e}{2(1 - e^2)^{1/2}}, \tag{3}$$

where

$$\alpha = \frac{\beta G M_\star}{r^2 c} \tag{4}$$

is referred to as the coefficient of dissipation. Note that $1/\alpha$ has the dimension of a time. Actually, it is the typical PR decay time scale for a and e. Finally, the total perturbation (1) has no effect on the orbital inclination i of the particles, since it lies in the orbital plane of the latter.

The values of the coefficients α and β for the Solar System are derived from Burns *et al.* (1979). These values can be scaled to the stellar mass and luminosity according to

$$\beta \sim \left(\frac{0.6Q}{s_{\mu m}\rho_{g\,cm^{-3}}}\right)\left(\frac{L_\star}{L_\odot}\right)\left(\frac{M_\odot}{M_\star}\right) \tag{5}$$

$$\alpha \sim \left(\frac{3.7 \times 10^{-4} Q}{s_{\mu m}\rho_{g\,cm^{-3}} a_{AU}^2}\right)\left(\frac{L_\star}{L_\odot}\right) \text{year}^{-1}, \tag{6}$$

where s, ρ, and a are the particle radius, density, and semimajor axis, respectively. Furthermore, Q is the radiation pressure efficiency, L represents the luminosity, $\odot$ refers to the Sun, and $\star$ refers to the star. The other subscripts indicate the units. Using $L_\star/L_\odot \sim 6$ and $M_\star/M_\odot \sim 1.5$, we have

$$\beta \sim \frac{2.4Q}{s_{\mu m}\rho_{g\,cm^{-3}}} \tag{7}$$

$$\alpha \sim \frac{2.2 \times 10^{-3} Q}{s_{\mu m}\rho_{g\,cm^{-3}} a_{AU}^2} \text{year}^{-1}. \tag{8}$$

The decay time due to PR drag is finally

$$t_{PR} = \frac{1}{\alpha} \sim \left(\frac{410}{Q}\right) \rho_{g\,cm^{-3}} s_{\mu m} a_{AU}^2 \text{ years}. \tag{9}$$

In the rest of this paper, we assume a density of the grains of 3 g cm^{-3}, typical of refractory materials like silicates. The coefficient Q lies in the range ~0.5–2 for μm-sized particles made of typical cosmic substances, while $Q = 1$ in the geometrical optics approximation (Burns *et al.* 1979).

The steady-state spatial density for dust particles evolving under PR drag only is proportional to r^{-q}, where $q = 1$ if the source is localized on a circular orbit, and where $q = 1.3$ if the sources are spread on eccentric orbits (Leinert and Grün 1990). As discussed previously, however, the distribution of dust around β Pictoris must present a central clearing zone to match the observations. Thus, such a distribution cannot be due to PR drag only.

Stellar wind induces a drag comparable to the PR drag. Actually, its effect can be modeled by introducing a multiplicative factor $1 + \text{sw}$ in front of the term $-\mathbf{v}/c$ in Eq. (1), where sw is the ratio of stellar wind drag to PR drag (Jackson and Zook 1992). This ratio is 0.3 in the case of the solar wind drag for magnetite grains in prograde orbits and 0.6 for retrograde orbits (Leinert and Grün 1990). As far as we know, we do not have information on this ratio in the more specific case of β Pictoris, or for other stars. Actually, this effect can be absorbed in the coefficients α or β, so that it does not alter our results. The stellar wind also induces a Coulomb pressure for charged particles due to passing stellar ions (Leinert and Grün 1990).

In the case of icy particles, the sputtering mechanism could be important: the pulling of atoms from the grain surface by the fast solar wind ions (Lanzerotti *et al.* 1978) could be an efficient mechanism to limit the presence of icy particles near the star.

The magnetic field also affects the motion of charged particles (Lorentz force). Note that a young star may have a strong stellar wind and/or a magnetic field, but we do not have in so far any observational constraints on that. The Lorentz force is important for very small particles (particles radius smaller than 0.1 μm in the Solar System, Leinert and Grün 1990).

The gas surrounding a young circumstellar disk can induce a drag on a particle. However, the circumstellar dust detected around α Lyrae, α Piscis Austrini, and ε Eridani does not show evidence for an important circumstellar gas component, in spite of a careful search (Hobbs 1986). The β Pictoris disk has only a very dilute gaseous component, with a hydrogen density of $\sim 10^4 - 10^5$ cm^{-3} at 400 AU (Norman and Paresce 1989). Because the mean free path of atoms is then much larger than the particle size, an Epstein drag acceleration acts on the particle (Weidenschilling 1977) of

$$\boldsymbol{\gamma}_{gas} = -\left(\frac{\rho_g}{\rho}\right)\left(\frac{v_T \mathbf{v}_r}{s}\right), \tag{10}$$

where ρ_g (resp. ρ) is the density of the gas (resp. the particle), v_T is the thermal velocity of the atoms, and $\mathbf{v}_r$ is the velocity of the particle relative to the gas. This drag causes an orbital decay of the particle at a rate of

$$\left(\frac{\dot{a}}{a}\right)_{gas} = -2\left(\frac{\rho_g}{\rho}\right)\left(\frac{v_T \mathbf{v}_r}{ans}\right), \tag{11}$$

where n is the mean motion of the particle, assumed to follow a circular orbit. The value of v_r is dominated by the fact that a particle orbits the star at a velocity $\sqrt{1-\beta}an$, due to the pressure of radiation, as explained after Eq. (1). Thus $v_r = -(1-\sqrt{1-\beta})an = \mathcal{O}(an\beta/2)$. Finally, a rough estimate of v_T is $\sim$1500 m sec^{-1}, assuming a temperature of $\sim$100 K for the gas at 20 AU. The value of ρ_g is the most difficult quantity to determine. There is no direct measurements of the neutral hydrogen number density n_H around β Pictoris, or around other stars with circumstellar dust disks. Indirect estimations can be made by the determination of ion densities such as AlII, CaII, MgII, FeII, etc., and then completion by hydrogen using typical interstellar abundances. The typical values, $n_H \sim 10^4 - 10^5$ cm^{-3} (Norman and Paresce 1989) are thus quite uncertain, especially because the hydrogen abundance may not be representative of interstellar values if the heavier elements are produced by already formed planetesimals or comets. The right-hand side of Eq. (11) is the inverse of the decay time t_{gas} due to the gas drag. Using $\rho = 3$ g cm^{-3} and the previous numerical values, one gets

$$t_{gas} \sim 4800 \left(\frac{10^4}{n_H}\right) s_{\mu m}^2 \text{ years}, \qquad (12)$$

where n_H is in cm^{-3}. Comparison of Eqs. (9) and (12) shows that, with a typical density of 10^4 cm^{-3}, the gas drag seriously competes with the PR drag for μm-sized particles. Note that this drag adds a new factor in the velocity dependent terms of Eq. (1), while the pressure of radiation remains the primary force which decides the orbital velocity of the particle around the star.

The sublimation of particles occurs at a distance from the star which depends on the particle composition. For most of the materials except ices, the melting temperature lies in the range 1000–1500 K. Hence, sublimation plays a role only at a few stellar radii from the star. According to Backman *et al.* (1992), sublimation of ice particles should be effective on a time scale much shorter than the stellar lifetime, inside a radius of $\sim$80 AU, i.e., the boundary between the outer and inner disks, which they have derived independently from IR and visible data. Thus, the grains that we consider in our model are assumed to be made of heavier elements, with typical density of 3 g cm^{-3}, as pointed out earlier.

The results of collisions between dust particles depends strongly on the impact velocity (Leinert and Grün 1990). The β Pictoris disk thickness increases linearly with the distance to the star, with full thickness of $\sim$30 AU at $\sim$100 AU (Norman and Paresce 1989), corresponding to an opening angle of $\sim$8°. This thickness implies typical impact velocities of $\sim$1 km sec^{-1} at 20 AU, more than sufficient to destroy the particles. The collision frequency, estimated from a normal optical thickness of $\tau \sim 5 \times 10^{-4}$ at 20 AU, is $t_{coll} \sim T_{orb}/8\tau \sim 2 \times 10^4$ years for an orbital period of 73 years, again at 20 AU (Backman *et al.* 1992). However, the figures used here being model dependent, the collisional time could easily vary by one order of magnitude.

We shall see that the total time scale for trapping into resonances, for the creation of accumulations of material or arc-like structures, and for the escape from the resonances lies in the range 10^5–10^6 years, against $\sim 10^4$ years for the collisional time scale. The structures excited by the resonances are thus expected to be continuously eroded, not only by the destructive collisions, but also by the various processes discussed in this section. The resulting steady state should then be a complex combination of several processes.

Our philosophy here is to *isolate* one of these processes, namely radiation forces acting together with resonant forcing from a hypothetical planet. Even though it may be argued that this does not necessarily describe the complete problem, or even the dominant forces, our approach can be validated for several reasons. (i) The intensity of radiation forces is quite robustly established. This study is thus applicable to a wide variety of stars with tenuous dust disks (with densities $\sim$10 times smaller than for the β Pictoris system), where all the other drags can be discarded. (ii) In contrast, gas drag, stellar wind drag, and magnetic forces depend on still poorly known parameters for most of these disks. (iii) Radiation forces may be viewed as an archetype of weak dissipative forces, with all the physics absorbed in one coefficient, β (or equivalently α; see Eqs. (5) and (6)). Studies of drags with similar forms, but different physical origins, could benefit from the present study. (iv) A mixture of various drags would obscure the main physics at work by adding new free parameters in the model.

Once the effects of one kind of force have been better understood, more complex physics can be included. For instance, the statistical distribution of dust that we obtain at a given moment can be used in a more sophisticated code, to study the collision frequency in various parts of the disk. Also, the gas drag can be implemented at little cost, in view of its similarity with the Poynting–Robsertson drag.

3.2. *Gravitational Perturbations*

A planet embedded in the disk can induce two kinds of gravitational perturbations:

(1) *Close encounters* of particles with the planet can lead to accretion, or to ejection of the particles on eccentric orbits. In this latter case, the pericenter or apocenter of the particle orbit remains near the planet orbit. Such a mechanism could in principle explain the inner clearing

zone if a large fraction of the infalling particles have close encounters with the planet. This happens if the radial migration of the particle between two encounters with the planet is less than the Hill radius of the planet, ah, where h is the Hill parameter $(m_p/3M_\star)^{1/3}$ and m_p is the mass of the planet. Assuming that the particle orbits in the same plane as the planet (2D case), some straightforward algebra then yields

$$\frac{m_p}{M_\star} > 3\left(\frac{16\pi}{3}\frac{\alpha}{n}\right)^{3/2}. \quad (13)$$

In the 3D case, however, there is an additional necessary condition, namely that the orbital inclination i of the particle be smaller than the Hill parameter h; i.e.,

$$\frac{m_p}{M_\star} > 3i^3. \quad (14)$$

Considering the value of α derived in Eq. (8), Eq. (13) is equivalent to $m_p/3M_\star > \sim 2 \times 10^{-7}/(s_{\mu m}^{3/2}\sqrt{a_{AU}^{3/4}})$. For particle sizes between 1 and 10 μm at 20 AU, this requires planet masses between $\sim 2 \times 10^{-5}\, M_\star$ and $7 \times 10^{-7}\, M_\star$. Thus, in the 2–D case, the planets that we consider (masses between 10^{-6} and $10^{-4}\, M_\star$, see Section 4.1) are large enough to scatter most of the particles through close encounters.

Using the second condition (14), we see that an Earth-like planet (mass $2 \times 10^{-6}\, M_\star$) is able to scatter particles through close encounters only if they have inclinations smaller than $\sim 0.5°$, while a Jupiter-like planet (mass $6.4 \times 10^{-4}\, M_\star$) can go up to $\sim 3.5°$. For this large mass, however, the planet is also able to trap particles into outer resonances well before they cross the planet orbit.

(2) *Mean motion resonances* induce long term perturbations on the particles. A pth order mean motion resonance occurs when the mean motions n_p and n of the planet and the particle are related by

$$(q + p)n_p - qn \sim 0, \quad (15)$$

where q is negative for exterior resonances and p is always positive. We will refer to the "$(q + 1):q$ resonance" for designating the above condition, for $p = 1$. When numerical values are used, we will drop the signs, without loss of information. For instance, when $q = -4$ and $p = 1$, we will refer to the 3 : 4 resonance.

The combination of dissipation (here, the PR drag) and resonance gives rise to a repulsive torque between the planet and the grain: particles at outer (resp. inner) resonances will gain (resp. lose) angular momentum. In that sense, only exterior resonances are able to halt the decay of particles. This mechanism is very general, and has been studied in the frame of planetary rings (Goldreich and Tremaine 1982, Greenberg 1983, Meyer-Vernet and Sicardy (1987), gas drag (Greenberg 1978, Weidenschilling and Davis 1985, Patterson 1987, Beaugé and Ferraz-Mello 1993, Kary *et al.* 1993), and PR drag (Gonczi *et al.* 1982, Jackson and Zook 1989, 1992, Sicardy *et al.* 1993, and Weidenschilling and Jackson 1993).

However, the problem of resonant capture with PR drag has difficulties of its own. First, the PR drag is not separable from the radiation pressure, which can significantly change the resonance locations, and thus their strength. Since the particle feels a star with an effective mass $(1 - \beta)M_\star$, Kepler's third law yields a resonant semimajor axis of

$$a_{res} = a_p(1 - \beta)^{1/3}\left(\frac{q}{q + p}\right)^{2/3} \quad (16)$$

for a $(q + p):q$ resonance. Another difficulty stems from the fact that the coefficient of dissipation associated with the PR drag is very small. This allows the particle to get high orbital eccentricities (e.g. ~ 0.5) before any equilibrium being reached. This yields analytical difficulties, linked to the crossing of the planetary orbit or nonlinear terms in the perturbing function (see Paper 2). So questions such as the existence and the stability of equilibrium orbits are much harder to answer than in the case of gas drag (Weidenschilling and Davis 1985).

4. THE MODEL

4.1. Physical Parameters

In our model, the dust particles are subjected to (i) the gravitational forces exerted by the star and a hypothetical planet orbiting it, (ii) the pressure of radiation, and (iii) the PR drag (Eq. (1)). The mass of the disk is neglected. The central star has a mass $M_\star = 1.5M_\odot$. The semimajor axis of the planetary orbit is fixed to 20 AU for all the runs, corresponding to an orbital period of $T_{pl} \sim 73$ years. The planetary mass m_p is a free parameter of our model, and is given in units of the stellar mass $M_\star$. Typical values in our model range from $10^{-6}\, M_\star$ to $10^{-4}\, M_\star$. For comparison, the Earth has a mass of about $2.0 \times 10^{-6}\, M_\star$, while Jupiter has a mass of $6.4 \times 10^{-4}\, M_\star$. These figures are $1.9 \times 10^{-4}\, M_\star$, $2.9 \times 10^{-5}\, M_\star$, and $3.4 \times 10^{-5}\, M_\star$ for Saturn, Uranus and Neptune, respectively. We thus explore the effects of planets from a small Earth up to a small Saturn. The other free parameters are the planet orbital eccentricity and the value of β.

The model is 3D; the initial inclinations of the particles to the planet orbital plane are randomly chosen between 0° and 8°. This figure corresponds to the estimated opening angle of the β Pictoris disk, as discussed earlier. However, several runs were carried out with zero inclinations (2D model), in order to better separate the role of the particle orbital inclinations in the trapping mechanism.

4.2. The Code

Our code is implemented on a Connection Machine CM-2/8k, a massively parallel computer. It can be described as a sample of microcomputers which all simultaneously execute the same instruction (SIMD computer), and which can exchange data on a very rapid network. Our model, which does not consider particle interactions, is thus particularly well adapted to the Connection Machine.

The code is described in more detail elsewhere (Scholl *et al.* 1993), and is briefly outlined here. Each particle is assigned to one of the 8192 microcomputers. This large number allows each run to reveal collective patterns on the disk driven by the planet, within a reasonable amount of CPU time (typically 6 hr for the integration of the motion of 8192 particles during 10,000 planet revolutions). The floating point accelerators implemented on the microcomputers have 32 bits (single precision). This limits the integration time to 10,000 planetary revolutions, a sufficient time scale for our purpose.

The code integrates the exact equations of motion in Cartesian coordinates, using a 4th order variable-time-step Runge–Kutta integrator. The latter is known to be comparatively slow on traditional monoprocessor computers. On a massively parallel computer, however, Runge–Kutta integrators are comparatively fast integrators. An intrinsic problem of parallel computing is to integrate a large number of orbits with a variable time step, since all the processors execute the same instructions. In principle, the particle which needs the smallest time step forces the other particles to proceed with an unnecessary slow scheme. One way out of this dilemna is an asynchronous use of the parallel computer. Each particle advances in time with its own, optimized, time step, and each particle has a different proper time during the run. The whole sample advances in time statistically at the same speed. In order to produce snapshots of the system at a prescribed time t_{pres}, the coordinates of a particle are stored when its proper time crosses t_{pres}.

A run is stopped when 80% of the sample has been integrated over 10,000 planetary revolutions. The position–velocity coordinates of the particles are kept every 500 planet periods (~36,500 years).

To follow the evolution of the particles for a longer time, some integrations of the exact equations of motion have been computed with double precision on a VAX 4500. This integration is done with a 4th order Bulirsch and Stoer integrator.

4.3. Initial Conditions

We use two kinds of initial conditions. (i) In most runs, the particles are initially randomly distributed on circular orbits with semimajor axes between 32 and 33 AU. This corresponds to a ring of particles which is far away from the first important outer resonance (1 : 2), near 28 AU. The next outer principal resonance (1 : 3) is located near 36 AU, but is ineffective for our selected range of planetary masses, eccentricities, and parameters β. All particles cross the 1 : 3 resonance without any significant change in the orbital elements. (ii) In another set of initial conditions, the particles have pericenter distances $a(1 - e)$ randomly distributed between 24 and 25 AU, a varying between 25 and 30 AU (Fig. 1a). This distribution corresponds to launching particles between 24 and 25 AU with various velocities. Otherwise, it is arbitrary (i.e., with no physical significance). However, it allows us to explore different values of initial eccentricity, an important parameter for the trapping into resonances. If need be, a subset of particles may be chosen in the initial population, in order to select a physically more relevant distribution.

We use β values of 0.1, 0.2, and mainly 0.3, corresponding to particle radii of 8, 4, and 2.7 μm, respectively, in the geometric optics approximation, and with $\rho = 3$ g cm^{-3} (Eq. (7)). However, various particle densities or optical properties are likely to be found in the disk. Consequently, these values of β should represent particles with sizes ranging roughly between 1 and 20 μm, a reasonable interval according to observations (Section 2). Values of β larger than 0.5 would lead to the escape of particles on hyperbolic orbits, for an initially circular Keplerian velocity (Burns *et al.* 1979). Values of β smaller than 0.1 require, on the other hand, an extremely long CPU time, since the decay time due to PR drag varies like $1/\beta$ (Eq. (9)).

Tables I and II list the values of the main parameters used in each run (C1 to C9 for the Connection Machine,

TABLE I

Simulations on the Connection Machine: 8192 Particles, 10,000 $T_{pl} \sim 7.3 \times 10^5$ years

run id.	planet mass[a]	planet orbit eccentricity	particle coeff. β	particle orbit inclinations[b]	particle orbit initial conditions[b]
C1	10^{-6}	0	0.3	0	$25 < a < 30,\ 24 < q < 25$
C2	10^{-4}	0	0.3	0	$25 < a < 30,\ 24 < q < 25$
C3	10^{-4}	0	0.3	0	$32 < a < 33,\ e = 0$
C4	10^{-6}	0	0.3	$0 < i < 8°$	$25 < a < 30,\ 24 < q < 25$
C5	10^{-4}	0	0.3	$0 < i < 8°$	$32 < a < 33,\ e = 0$
C6	10^{-4}	0.01	0.3	0	$32 < a < 33,\ e = 0$
C7	10^{-5}	0	0.3	0	$25 < a < 30,\ 24 < q < 25$
C8	10^{-5}	0	0.1	0	$25 < a < 30,\ 24 < q < 25$
C9	10^{-4}	0	0.3	$0 < i < 8°$	$25 < a, 24 < q,\ e < 0.333$

[a] In units of the stellar mass.

[b] When an interval is specified, the quantity is randomly chosen in that interval. The quantities a, e, i, and q are respectively the semimajor axis, the eccentricity, the inclination, and the pericentric distance. Distances are in AU.

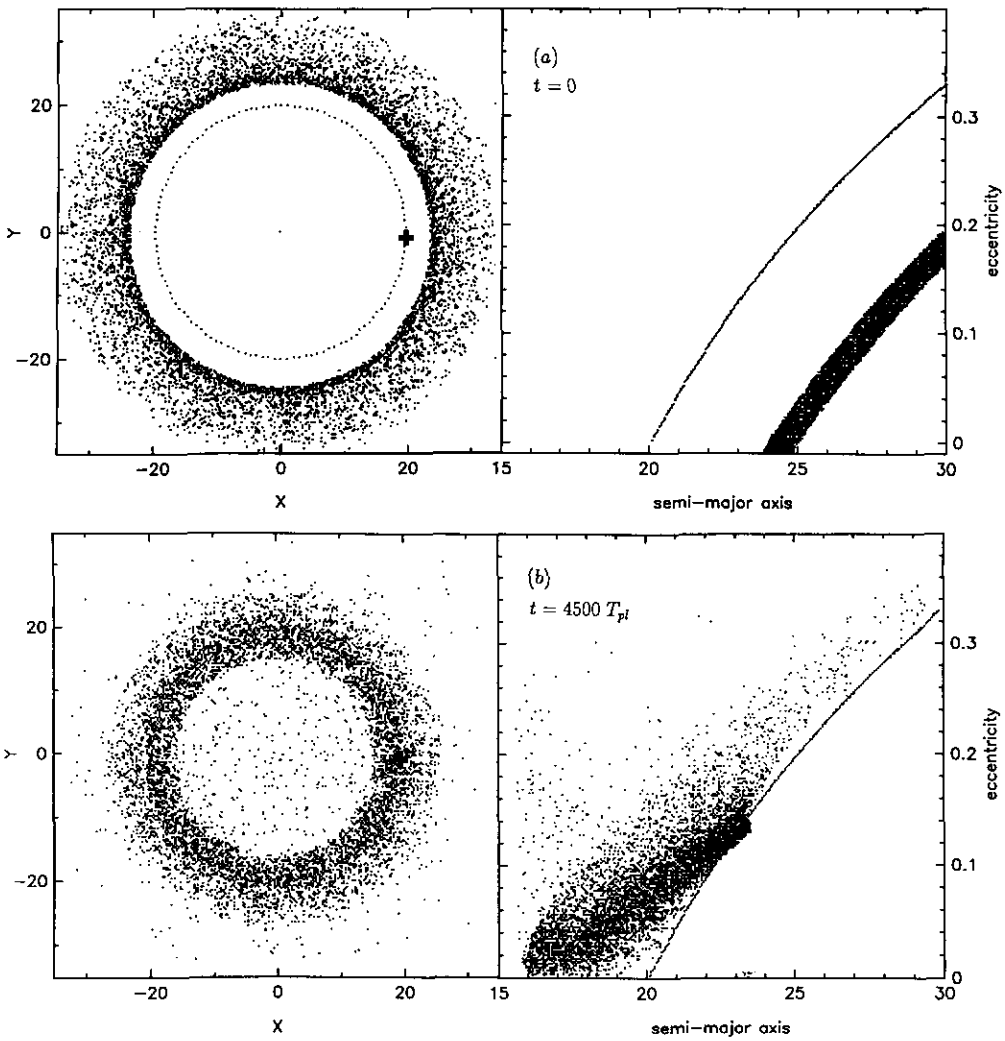

FIG. 1. *Left panels:* Pole-on view of the simulated circumstellar dust disk. The central star, representing β Pictoris, has a mass $M_\star = 1.5\ M_\odot$. The dotted line is the orbit of the planet, at 20 AU from the star. The particle positions are plotted in a frame corotating with the planet (marked as a cross), whose mass is here $10^{-6}\ M_\star$, i.e., ~0.5 Earth mass. Orbital motion is counter-clockwise, and one planetary revolution takes ~73 years. In all figures, distances are in astronomical units (AU). *Right panels:* Eccentricity vs semimajor axis, or (a, e) diagrams. The solid line represents the points of constant pericenter distance, $a(1 - e) = 20$ AU. Above that curve, the particle orbits cross the planetary orbit. The parameters of this run (C1) are summarized in Table 1. (a) Initial conditions. (b) The system after 4500 planetary revolutions T_{pl} (3.3×10^5 years).

and V1 to V3 for the VAX 4500), and provide the identification labels which are used later in the paper.

5. RESULTS

5.1. 2D Disk with Circular Planetary Orbit

With an *Earth-like* planet with mass $10^{-6}\ M_\star = 0.5$ Earth mass (model C1, see Table I), all the particles, which have zero inclinations, fall onto the star at the rate given by Eq. (9), with $\beta = 0.3$, and $1/\alpha \sim 4.4 \times 10^6$ years. There is no trapping at resonances; the only action of the planet is to scatter the particles through close encounters (Fig. 1), as expected from Eq. (13) and the following discussion. The particles are ejected either inside or outside the planet orbit, with their pericenters or apocenters at the planet orbital radius (20 AU). This is readily visible in Fig. 1b, where the points are scattered parallel to the curve $a(1 - e) = 20$ AU in the (a, e) diagram.

With a larger, *Uranian-like* planet of mass $10^{-4}\ M_\star \sim$ 0.5 Saturn mass (model C2), all the particles decay until they reach a resonance (Fig. 2). Then they are trapped for a time span comparable to or larger than the decay time scale, which explains the accumulations observed in the (a, e) diagram. The first order resonances 1 : 2, 2 : 3, and 3 : 4 are the most effective ones, but second order

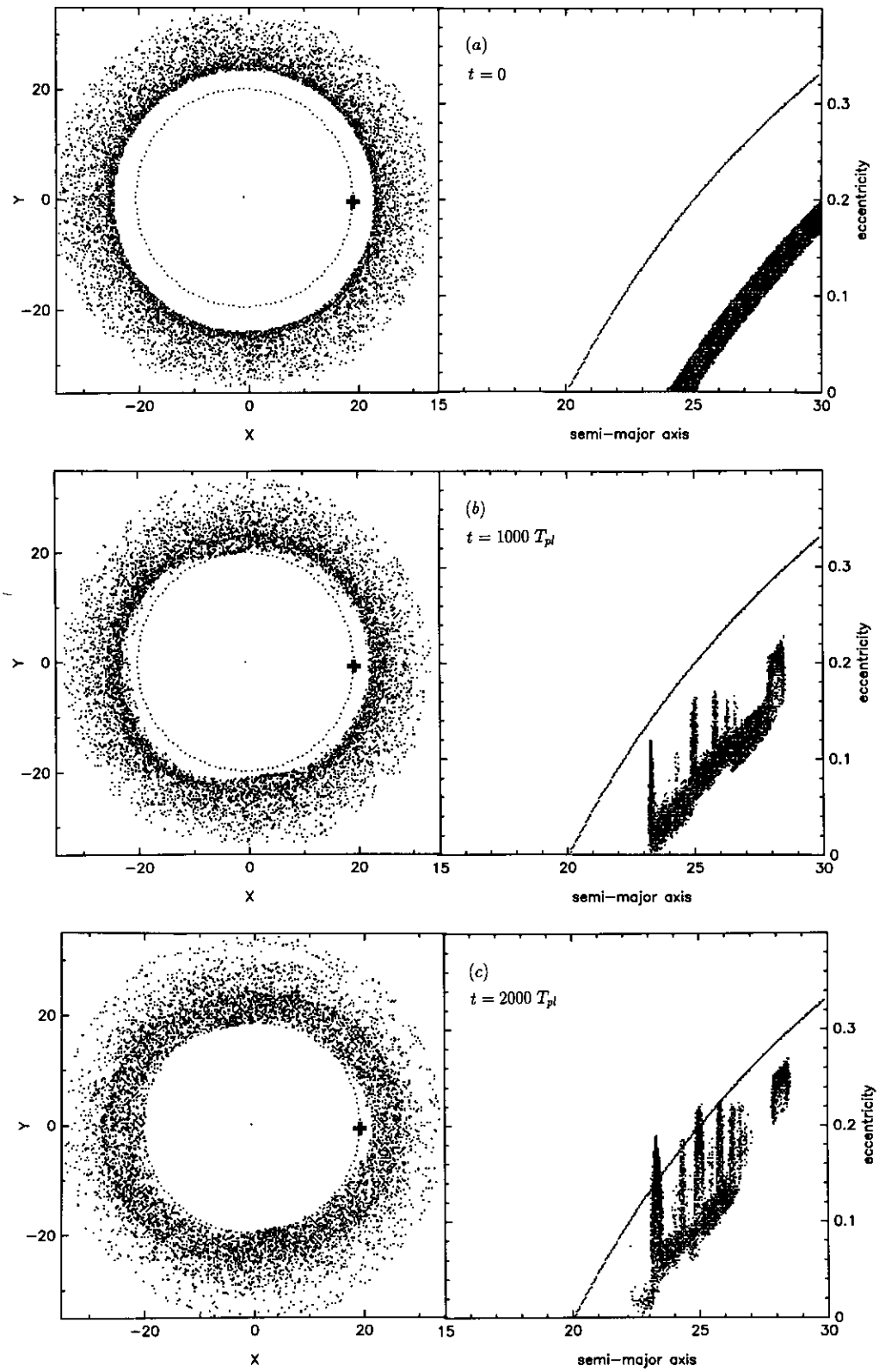

FIG. 2. The parameters of this run (C2) are given in Table I. The planetary mass ($10^{-4}\ M_{\star}$) corresponds to ~50 Earth masses, or ~0.5 Saturn mass. The model is 2D; i.e., all the particles lie in the planetary orbital plane. (a) Initial conditions. (b–i) The system every 1000 planet revolutions (7.3×10^4 years). The panel (g) is the same time step as panel (f), but at a different scale. The last time step (i) is at 7000 T_{pl} (5.11×10^5 years). Some resonance locations are indicated in the right panel (e).

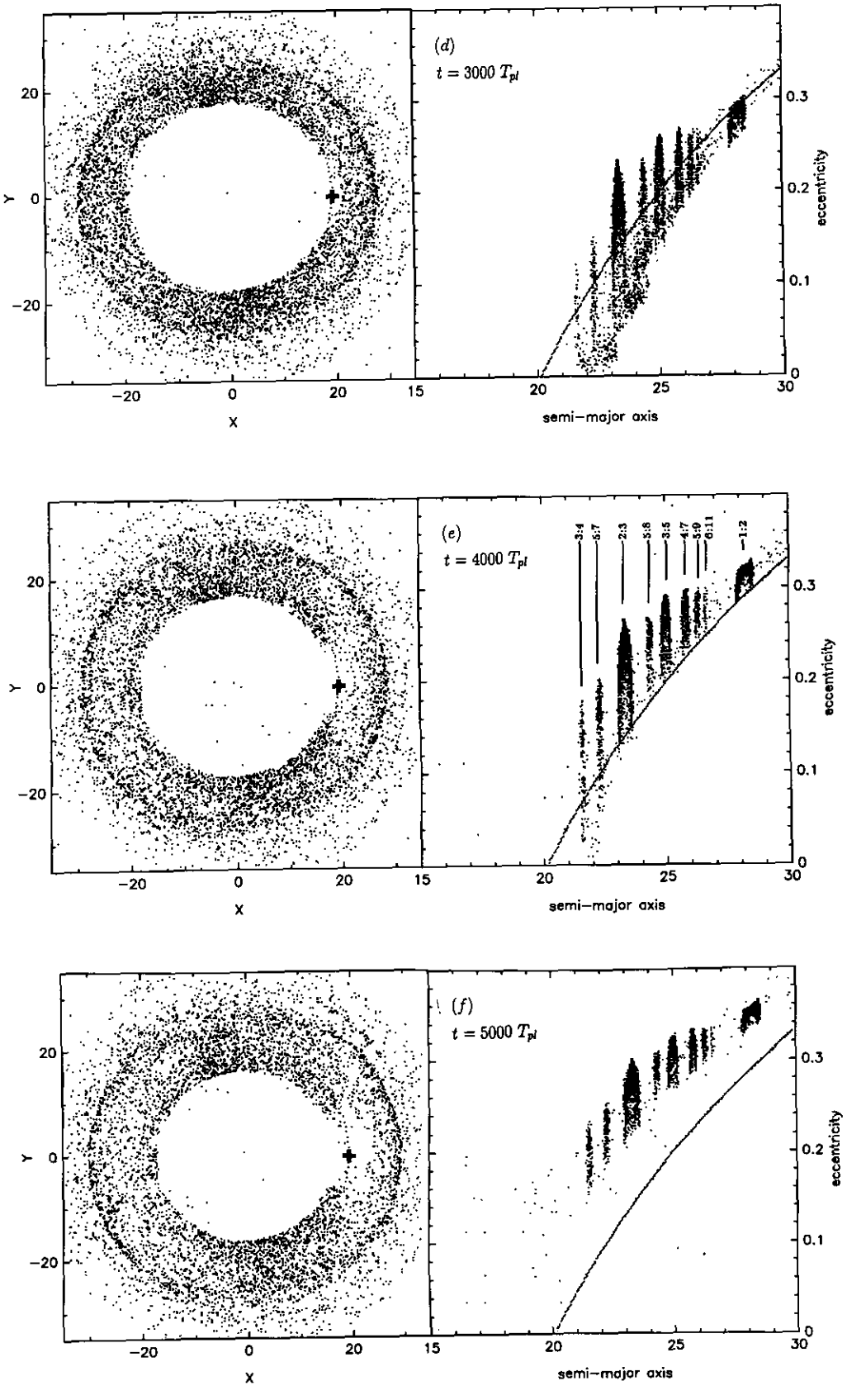

FIG. 2—*Continued*

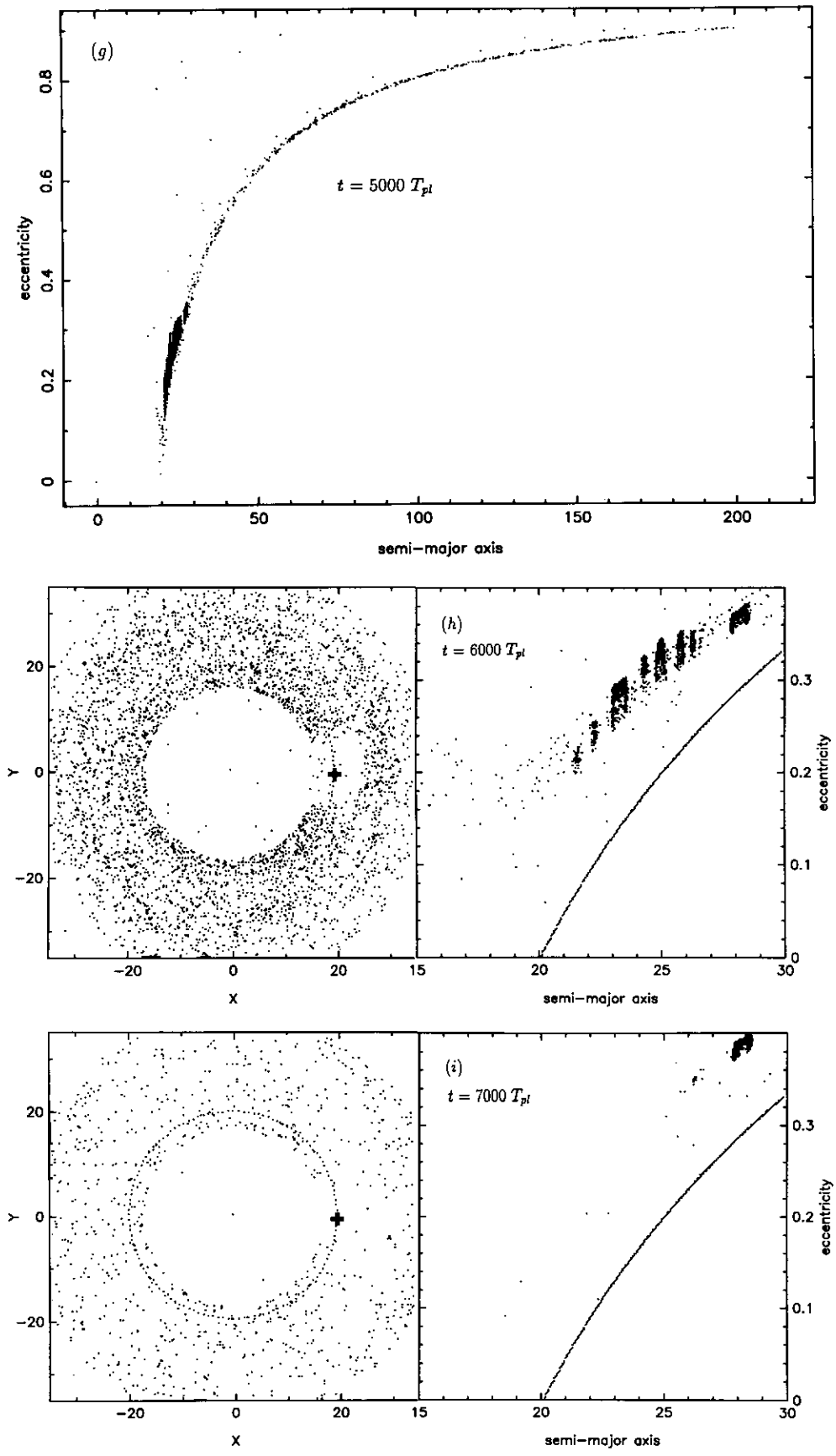

FIG. 2—*Continued*

TABLE II
Simulations on the Vax 4500: One Particle, Double Precision

run id.	planet mass	planet orbit eccentricity	particle coeff. β	particle orbit inclination	particle orbit initial condition
V1	10^{-4}	0	0.3	0	$a = 30.$ $e=0$
V2	10^{-4}	0	0.3	8°	$a = 30.$ $e=0$
V3	10^{-4}	0.01	0.3	0	$a = 30.$ $e=0$

Note. See Table I for definitions.

resonances (e.g., 3 : 5 at 24.96 AU), third order resonances (4 : 7 at 25.79 AU, and 5 : 8 at 24.29 AU), fourth order resonances (5 : 9 at 26.28 AU), or even higher order resonances can also trap particles (Fig. 2e) In Figs. 2c to 2g, the particles trapped in the 2 : 3 resonance are particularly visible, as they are distributed on two-lobe trajectories. Also, accumulations of particles near periapses, at $-70°$ and $+110°$ from the planet, are clearly visible.

More generally, each $(q + 1) : q$ resonance will force a motion yielding a trajectory with $|q + 1|$ lobes, in the frame corotating with the planet. Note that the resonances are well isolated in the (a, e) diagram. However, due to the superpositions of various trajectories corresponding to various resonances, and owing to the large eccentricity of each orbit, these $|q + 1|$-lobe trajectories are mixed in the physical space. The resulting distribution (see for instance Fig. 2f) shows residual accumulations at $-70°$ and $+110°$ from the planet. It also exhibits a void of matter around the planet, and corotating with it. This void is caused by the resonances, which all tend to align the apoapses of the particle orbits with the star–planet line (this mechanism being sometimes referred to as the protection mechanism).

Finally, note that the inner region of the disk is sparsely populated, even at the end of the run. This is due to the fact that decay time scales are reduced, once the particles have had a close encounteder with the planet, and have thus acquired higher orbital eccentricities. This point will be discussed again in Section 5.6.

Until $t = 6000\ T_{pl}$ ($\sim 4.4 \times 10^5$ years, see Fig. 2h), almost all the particles are locked in a resonance. At this stage, only ~ 1000 particles, out of 8192, have had a close encounter with the planet and have been ejected. The particles ejected outside the planetary orbit have semimajor axes as large as 200 AU, and their pericenters remain at the planetary orbit, i.e., $a(1 - e) \sim 20$ AU (Fig. 2g). At $T = 7000\ T_{pl}$, 8000 particles have been ejected from the resonances, and at $t = 8000\ T_{pl}$ ($\sim 5.8 \times 10^5$ years), all the particles have been removed from the resonances.

In order to better understand the evolution of the particles in a given resonance, we now consider a simulation where all the particles are initially in circular orbits outside the 1 : 2 resonance (model C3, see Fig. 3). At the crossing of the 1 : 2 resonance (28.2 AU for $\beta = 0.3$), all the particles are trapped, and their semimajor axes oscillate around the resonance radius, while their eccentricities increase (Figs. 3-b,c). The small oscillations are due to the fact that the eccentricity vectors of the particles tend to follow the curves corresponding to the local conservation of the Jacobi constant ($de^2 \propto da$), while the dissipation monotonically changes this Jacobi "constant." This point is analyzed in detail in Paper 2. When the particle's eccentricity increases, the rate of increase decreases. After 10,000 T_{pl}, the run is stopped and all the particles are still trapped with eccentricities ~ 0.4. Double precision runs carried out with one particle on a Vax 4500 allow one to see that the particles which start from 30 AU on circular orbits remain trapped for almost 22,000 planetary periods (1.6×10^6 years) before escaping the resonance (see Fig. 6 and Section 5.4).

At a certain stage, the large eccentricity allows the particles to cross the planet orbit. Nevertheless, close encounters are avoided because of the resonance protection mechanism: the particle pericenters oscillate around a mean position which avoids the planet (Fig. 3c). An individual particle then follows a trajectory similar to that described by Jackson and Zook (1989) in the case of a capture of a grain into a resonance with the Earth. With the large number of particles, this gives rise to a wave pattern trailing the planet with an angle $\sim -80°$ and corotating with it.

This angle is related to the resonant angle $\Psi_L \equiv (q + 1)\lambda_p - q\lambda - \tilde{\omega}$, where λ (resp. λ_p) is the mean longitude of the particle (resp. the planet), and $\tilde{\omega}$ is the longitude of the pericenter of the particle orbit. The subscript L refers to Lindblad resonance, as opposed to corotation resonance; see Section 5.3. For the 1 : 2 resonance, $q = -2$, so that $\Psi_L = \tilde{\omega} - \lambda_p$ when a particle reaches its pericenter. In this case, the average angle of $-80°$ visible in Fig. 3c coincides with the value of Ψ_L. The "pretzel" shape obtained here is particular to the 1 : 2 resonance. More generally, a swarm of particles locked in a $(q + 1) : q$ resonance exhibits a flower-shaped pattern with $|q + 1|$ petals, avoiding the planet and corotating with it. The energetics of the resonance requires that Ψ_L be negative, to compensate for Poynting–Robertson drag energy loss (see Paper 2 and references therein).

5.2. *3D Disk with a Circular Planetary Orbit*

The particle inclinations are now distributed between 0° and 8° with respect to the planetary orbital plane. A planet with a mass of $10^{-6}\ M_\star$ (run C4) has almost no influence on a thick disk. In contrast to the 2D run shown in Fig. 1, where almost all the particles had a close encoun-

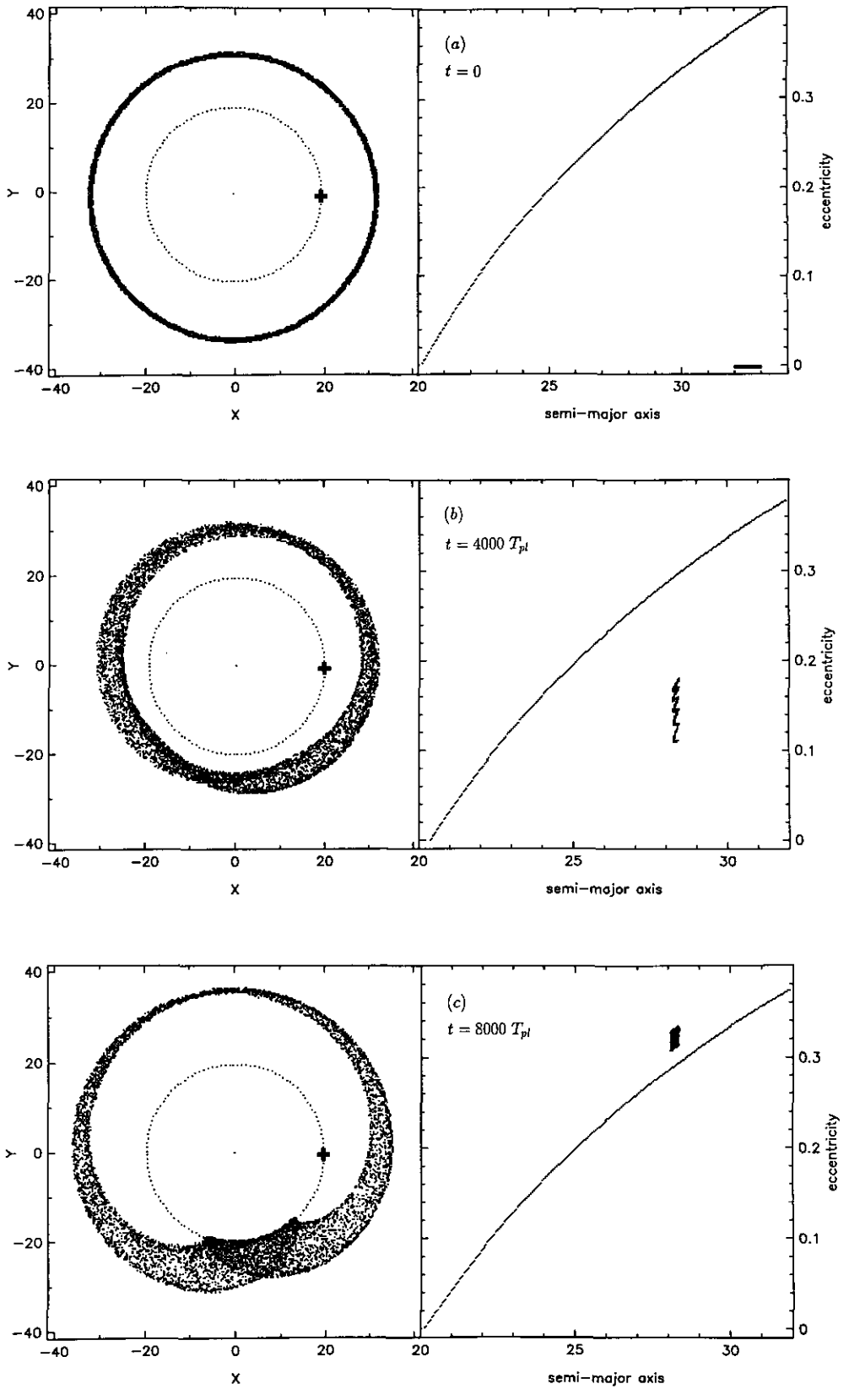

FIG. 3. Same as Fig. 2, except for the initial conditions: the particles are initially in *circular* orbits between 32 and 33 AU (model C3 in Table I). (a) Initial conditions. (b) The system after 4000 T_{pl} (2.92×10^5 years). (c) the system after 8000 T_{pl} (5.84×10^5 years).

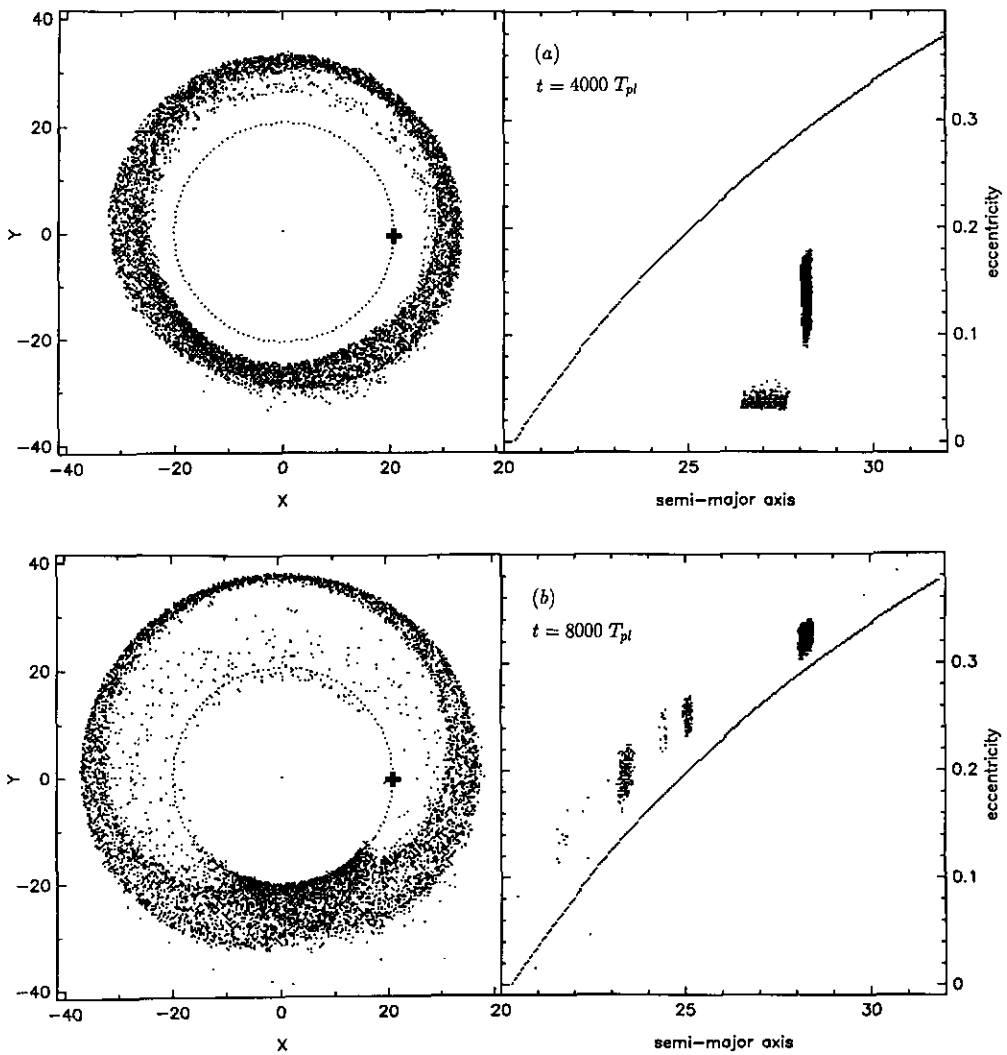

FIG. 4. Same as Fig. 3, except that the disk is now 3D. Particles have initial inclinations randomly distributed between 0° and 8° (model C5 in Table I). (a) The system after 4000 T_{pl} (2.92×10^5 years). (b) The system after 8000 T_{pl} (5.84×10^5 years).

ter with the planet, the inclined particles are little perturbed, as expected from Eq. (14). In this case, only 5% of them have had a close encounter and been ejected. Thus, the scattering effect of a planet could be important only for a very flat disk.

We consider now a planet with mass $10^{-4} M_\star$, the other parameters being the same as in the previous section (run C5). The main difference from the planar model is that about 5% of the particles escape the 1 : 2 resonance, when their eccentricities are between 0.037 and 0.06 (Fig. 4a). These particles continue their fall until they reach higher q resonances, closer to the planet (Fig. 4b). The particles escaping the 1 : 2 resonance are the more inclined ones: about 20% of the particles with inclination between 6° and 8° actually escape the resonance. The inclinations of the particles trapped into the resonance are not statistically increased, in contrast to the eccentricities. Thus, the thickness of the disk is not increased by the resonance mechanism.

At the end of the 10,000 T_{pl} integration, a large number of particles are still trapped in the resonance, in contrast to the 2D case, where all the particles are ejected after 8,000 planet period. The computation of one-particle motion with an inclination of 8° (model V2 of Table II) shows that ejection from the resonance occurs at an eccentricity similar to the 2D case, that is, ~0.5.

Once trapping into resonance occurs, the eccentricity first increases rapidly, and then slows down as it approaches a limiting value. The analysis carried out in Paper 2 shows that the eccentricity first varies like $\sqrt{t}$, where the time is counted from the entrance into the resonance. As illustrated in Fig. 4a or 5a, in the case of the 1 : 2 resonance, particles which enter the resonance can escape from it at eccentricities lower than ~0.07.

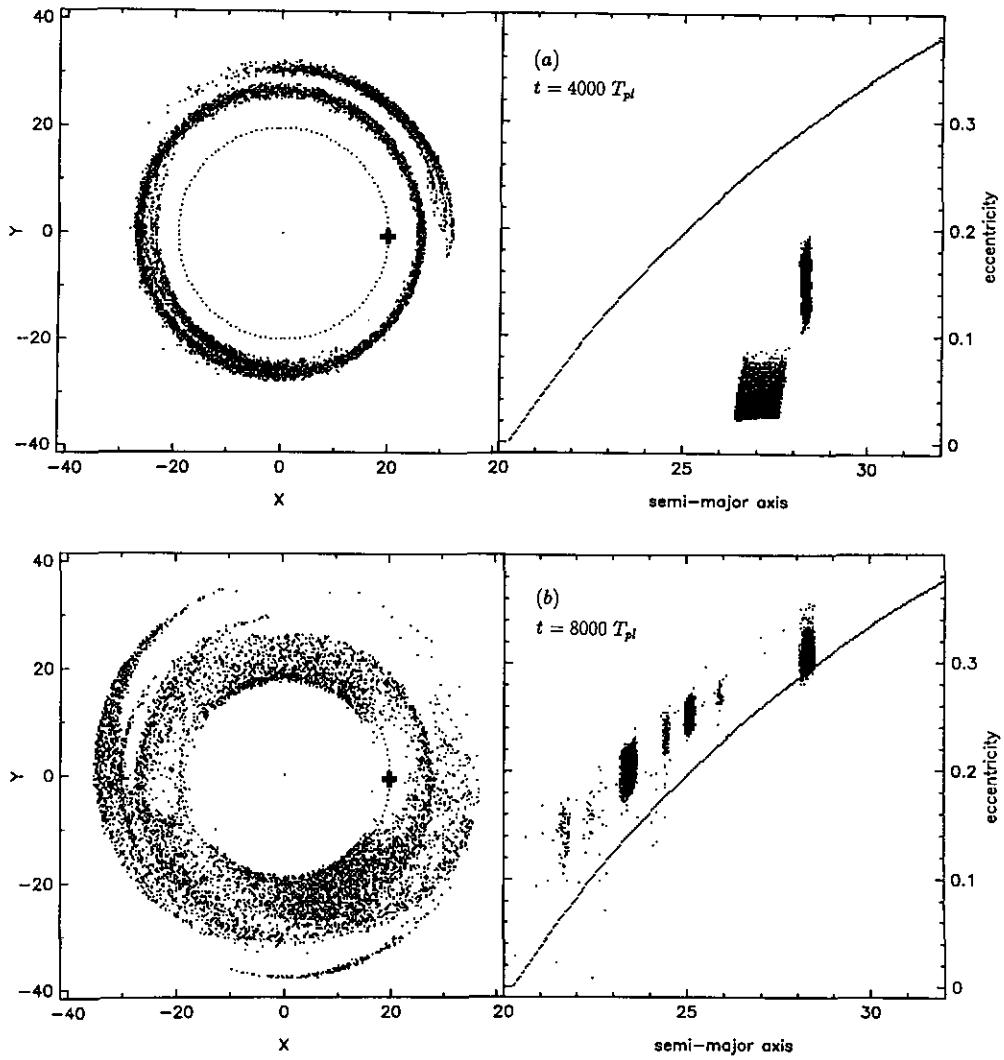

FIG. 5. Same as in Fig. 3, except that the planet has an orbital eccentricity of 0.01. The parameters are given in Table I (model C6). (a) The system after 4000 T_{pl} (2.92×10^5 years). (b) The system after 8000 T_{pl} (5.84×10^5 years).

Above that value, the particles remain locked in the resonance, and the eccentricities increase at a decreasing rate. An eqilibrium value e_{eq} is in principle possible, for which the energy dissipated by PR drag is exactly compensated by the energy provided by the planet. The value of e_{eq} is estimated in Paper 2 for first order resonances. The question of the stability of these equilibria is analyzed further in Section 5.4.

5.3. 2D Disk with Eccentric Planetary Orbit

We consider now a planet with an orbital eccentricity of 0.01. The other parameters are given in Table I (run C6).

With an eccentric planetary orbit, the trapping into the 1:2 resonance is not as efficient as with a planet in a circular orbit: almost half the particles escape the resonance even though they lie in the planetary orbital plane (Fig. 5a). However, they are trapped in higher q resonances (Fig. 5b). At the end of the 10,000 T_{pl} integration, the particles are still trapped in the resonance. A computation of one-particle motion in double precision (run V3, Table II) shows that ejection occurs at an eccentricity of 0.56, which is larger than the equilibrium eccentricity computed analytically for a circular planetary orbit, which is 0.51 (see Eq. (17) and Paper 2).

The particles trapped in the 1:2 resonance form two arc-like structures, which corotate with the *particles*, not the planet (Fig. 5b). Otherwise, they evolve along the pretzel-shaped curve shown in Fig. 3c. Actually, two kinds of resonances are now at work: a *Lindblad* resonance, associated with the resonant angle $\Psi_L = (q + 1)\lambda_p - q\lambda - \tilde{\omega}$, and a *corotation* resonance, associated

with the angle $\Psi_C = (q + 1)\lambda_p - q\lambda - \tilde{\omega}_p$, where $\tilde{\omega}_p$ is the longitude of the planetary pericenter. The Lindblad resonance excites the particle orbital eccentricity, while the corotation resonance traps the particle in $|q|$ intervals of longitude.

This arc forming mechanism has been studied in the frame of planetary ring arc dynamics (Goldreich *et al.* 1986, Sicardy 1991, Porco 1991). It also bears resemblance to the arc structures found by Patterson (1987), where the particles are submitted to a gas drag in the solar nebula, and are perturbed by a Jovian planet on an elliptic orbit. As seen in Fig. 5b, even a moderate eccentricity of the planet induces conspicuous azimuthal asymmetries in the disk. Note also the depleted region in front of the planet. It is caused by the protection mechanism associated with various Lindblad resonances, as discussed in Section 5.1. Thus, in contrast to the arc structures, this depleted region corotates with the planet.

5.4. *Temporary or Permanent Trapping?*

We have seen that if the particles can reach a critical eccentricity (roughly 0.07 for the 1 : 2 resonance; see Fig. 4a), then they remain trapped for a long time until they reach a high eccentricity leading to planetary orbit crossing. Several questions are then in order: Is the trapping permanent? Is there an equilibrium orbit? Is it stable? If not, what is the typical trapping time?

Existence of an equilibrium eccentricity. Analytical approaches indicate that the eccentricity can reach an equilibrium value of e_{eq}, for which all the energy provided by the planet is exactly dissipated through PR drag. The value of e_{eq} depends on the q of the resonance, but *not* on the dissipation coefficient α, nor on the planetary mass. This surprising result is discussed by Weidenschilling and Davis (1985), Beaugé and Ferraz-Mello (1993), Sicardy et al. (1993), and in Paper 2. The value of e_{eq} is given by (Paper 2)

$$(q + 1)(1 + e_{eq}^2) = q(1 - e_{eq}^2)^{3/2}, \qquad (17)$$

which shows that $e_{eq} = 1/\sqrt{f|q|}$, where f depends weakly on q, and tends to 2.5 for large q's. For the 1 : 2 resonance examined in the next paragraph, $e_{eq} \sim 0.51$.

Stability of the equilibrium eccentricity. The question of the stability of the equilibrium orbit is, however, a more difficult matter. Figure 6 shows the motion of a single particle in the (a, e) diagram and in the eccentricity vector $(e\cos(\Psi_L), e\sin(\Psi_L))$ diagram. The parameters are given in Table I (run V1). The particle is trapped into the 1 : 2 resonance for as long as 20,000 planet revolutions ($\sim 1.4 \times 10^6$ years). In a first stage, the eccentricity increases, approaching e_{eq}. Then, near $e_{eq} \sim 0.51$, the amplitude of oscillations in a increases (Fig. 6a), and the particle suddenly escapes the resonance and undergoes a close encounter with the planet.

Fig. 6b analyzes the behavior of the eccentricity vector $(e\cos(\Psi_L), e\sin(\Psi_L))$. The dotted curve on the right represents the locus of points where the particle has an encounter with the planet. The protection mechanism ensures that near $\Psi_L = 180°$, there is no value of eccentricity for which the particle can have an encounter. The eccentricity vector first oscillates in a libration motion with a small amplitude, and the resonant argument near 80°. When the eccentricity is about to reach the value e_{eq}, the amplitude of libration of the eccentricity vector suddenly increases, so that the particle gets closer to the "dangerous" dotted curve corresponding to encounters. Then, Ψ_L moves and oscillates around 80°. The eccentricity reaches 0.47 and the particle escapes the resonance. The study of the exterior resonances phase space shows that, at a certain energy level, the libration curve splits into two regions centered on $-80°$ and 80° (Beaugé 1993).

Figure 6c corresponds to the same simulation where the drag parameter β has been set equal to zero at different steps of the previous simulations, that is, when the particle eccentricity reaches 0.1, 0.2, 0.3, 0.4, and 0.46. Then the eccentricity vector evolves on the "osculating" libration curve (see Paper 2, where this technique is described in detail). Figure 6c shows that, until $e = 0.3$, the libration curve is symmetrical with respect to the horizontal axis and becomes narrower and narrower as e increases. For large eccentricities, the osculating libration curve becomes small and asymmetrical, centered on 80°. In other runs, not shown here, with different initial phase of the particle, the particle escapes the resonance when the amplitude of Ψ_L becomes large, before Ψ_L evolves to 80°.

As far as we know, there is no analysis yet of the escape mechanism near e_{eq}. Some comments on this points are made in Paper 2. The behavior shown in Fig. 6 is quite archetypal. In fact, we have *not* observed any permanent trapping during any of our integrations. More precisely, we have not observed any attracting equilibrium orbits. That is at variance with the results of Greenberg (1978), Weidenschilling and Davis (1985), Patterson (1987), and Beaugé and Ferraz-Mello (1993). In these latter cases, however, the physics of dissipation is different, since it is associated with gas drag, not PR drag. The larger value of the dissipation coefficient in the case of gas drag damps the eccentricity more efficiently. This prevents orbit crossings, and allows the particles to reach stable equilibrium orbits. More work is now needed to understand the behavior shown in Fig. 6, and in particular the outcomes of close encounters with the planet. Some estimates of the trapping time scale can nevertheless be given, as we see now.

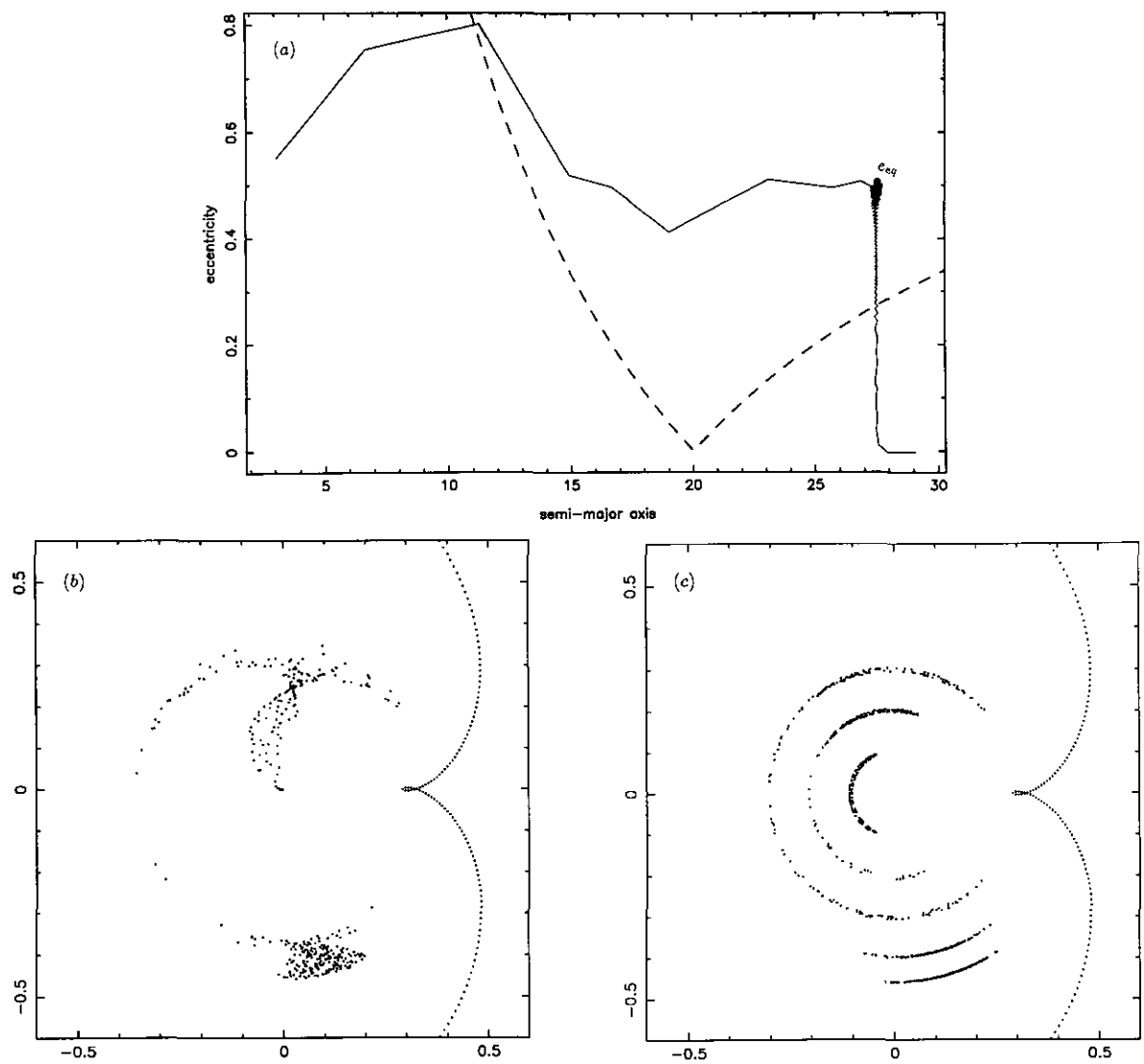

FIG. 6. Evolution of one particle. The parameters are given in Table II (model V1). In this case, the particles are trapped for 1.6×10^6 years ($\sim$ 22,000 T_{pl}) before escaping from the resonance. (a) Evolution of the system in the (a, e) diagram. There is one point every 100 planetary revolutions (7300 years). The value of the equilibrium eccentricity e_{eq}, calculated from Eq. (17), is also indicated, see text for details. The left branch of the dashed curve represents the orbits with constant apocenter distance, $a(1 + e) = 20$ AU, while the right branch represents constant pericenter distance $a(1 - e) = 20$ AU. Points above the dashed curve correspond to trajectories crossing the planetary orbit. (b) Evolution of the eccentricity vector $e \cos(\Psi_L)$, $e \sin(\Psi_L)$, where Ψ_L is the Lindlad resonance argument. The dotted curve represents the points where the particles has an encounter with the planet; see the text for details. (c) Evolution of the eccentricity vector if the Poynting–Robertson drag is stopped when the particle eccentricity is 0.1, 0.2, 0.3, 0.4, or 0.46; see the text for details. There is one point every 20 planet revolutions (1460 years).

Trapping time scale. The variation of eccentricity with time is estimated in Paper 2. If the eccentricity starts from zero at the entrance into the resonance, and while it is still small with respect to e_{eq}, it varies as

$$e(t) = \sqrt{\frac{2\alpha t}{|q|}}. \tag{18}$$

Using the value $\beta = 0.3$, i.e., $\alpha \sim 6.9 \times 10^{-7}$ years^{-1} (Eqs. (7) and (8)), and for instance $t = 8000\ T_{pl}$ ($\sim 5.8 \times 10^5$ years) and $q = -2$, one gets $e \sim 0.63$. One can see in Fig. 3c that this overestimates the eccentricity at that time by a factor of $\sim$2. This is expected because the rate of change of e slows down, with respect to Eq. (18), when equilibrium is approached; see Weidenschilling and Jackson (1993). Another test of Eq. (18) is provided by

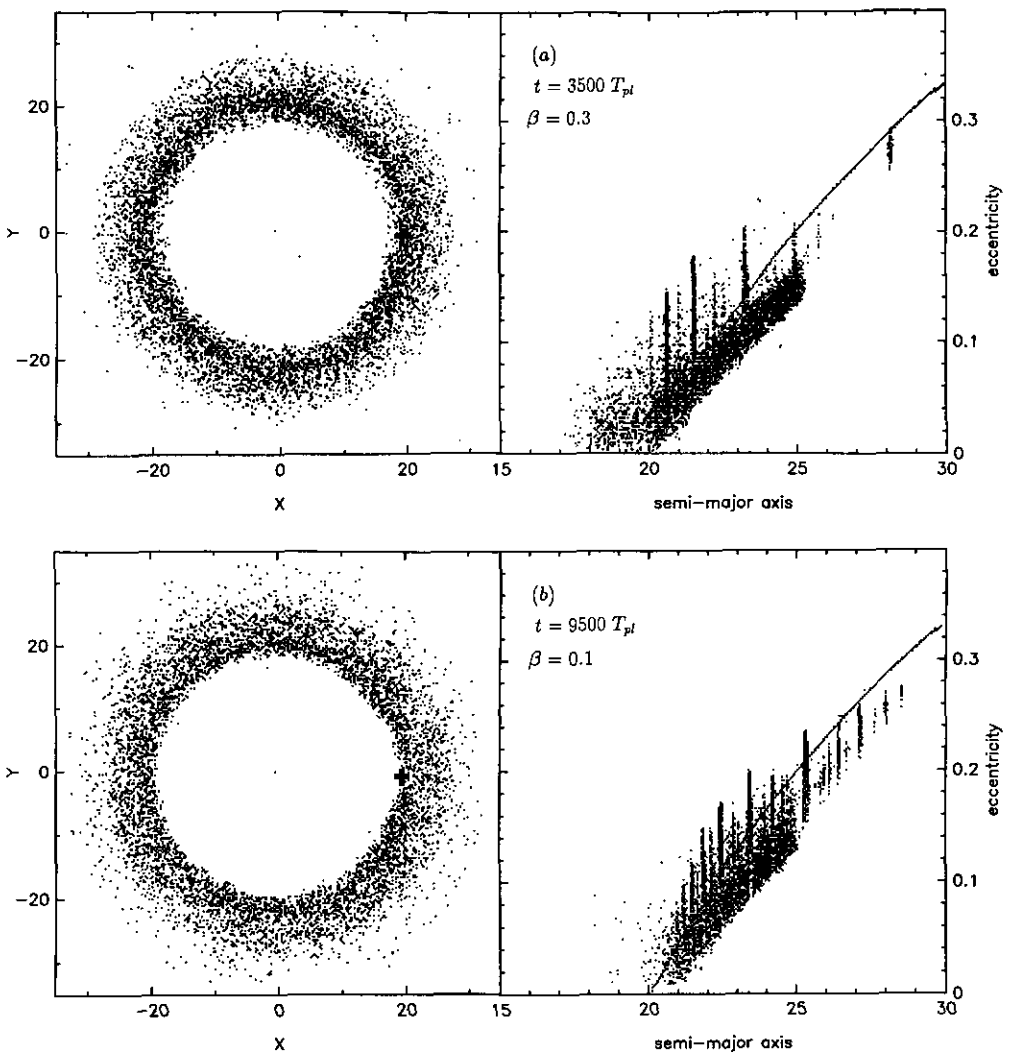

FIG. 7. Effect of the variation of β, with $10^{-5}\ M_\star \sim 5$ Earth masses fixed. (a) $\beta = 0.3$, the system after 3500 planetary revolutions (2.56×10^5 years, model C7, see Table I). (b) $\beta = 0.1$, the system after 9500 planetary revolutions (6.94×10^5 years, model C8).

Fig. 7. The time it takes to reach a given eccentricity is expected to be proportional to $1/\alpha$, and thus, also to $1/\beta$. Since the two runs of Figs. 7a and 7b are made with $\beta = 0.3$ and $\beta = 0.1$, respectively, it should take three times as long to reach the same eccentricity in the second case, in good agreement with the results shown in this figure.

A rough estimate of the trapping time is obtained by calculating the time t_{trap} it takes the eccentricity e to reach the equilibrium value $e_{\text{eq}} \sim 1/\sqrt{2.5|q|}$ (Eq. (17)). Assuming Eq. (18) holds all way through, this yields

$$t_{\text{trap}} \sim \frac{1}{5\alpha}. \tag{19}$$

One must remember that this is a *lower* bound, since the variation of e is slower than expected from Eq. (18) when approaching e_{eq}. The run V1 (Fig. 6) gives a trapping time of twice this value for the 1 : 2 resonance.

Thus, even if not permanent, the trapping time is comparable to the PR decay time $1/\alpha$, i.e., $\sim 10^6$ years for μm-sized particles. In that sense, resonance trapping may be an efficient way for accumulating material outside the planet orbit; see Section 5.8.

Note finally that the trapping time t_{trap} is expected to be *independent* of q. This is actually confirmed by our simulations: the particles are ejected from the resonances at about the same time; see, e.g., Fig. 2. Note also that the eccentricity e and t_{trap} are *independent* of the planet mass. This is confirmed again by our runs: for instance, in Fig. 8, we see that for planetary masses of 10^{-5} and $10^{-4}\ M_\star$, about the same eccentricities are reached at the same time, i.e., 4500 T_{pl}.

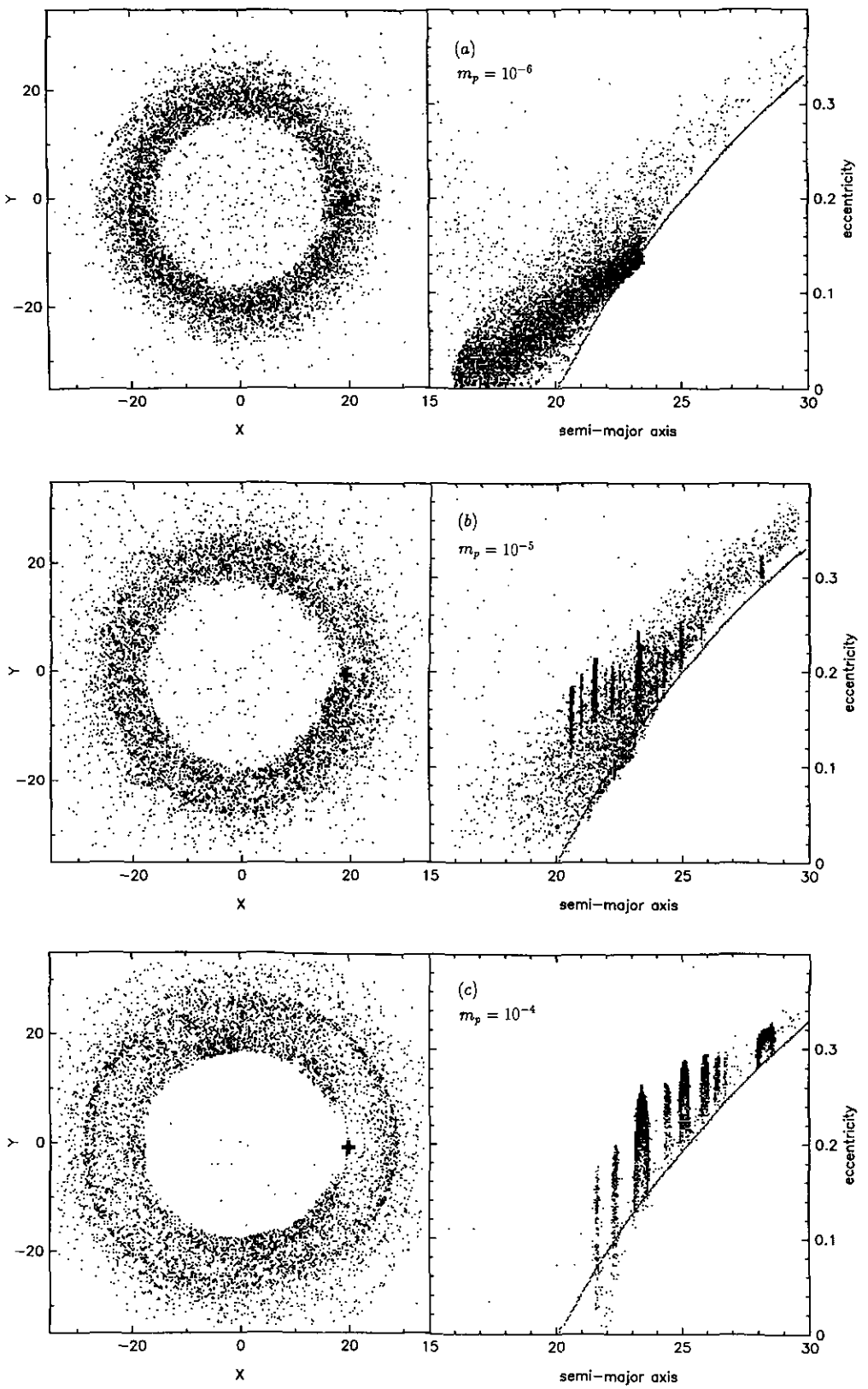

FIG. 8. Variation of the planet mass. Each panel shows the system after 4500 planetary revolutions (3.29×10^5 years), with various planet masses m_p: (a) $m_p = 10^{-6} M_\star \sim 0.5$ Earth masses (model C1, see Table I). (b) $m_p = 10^{-5} M_\star \sim 5$ Earth masses (model C7). (c) $m_p = 10^{-4} M_\star \sim 50$ Earth masses (model C2).

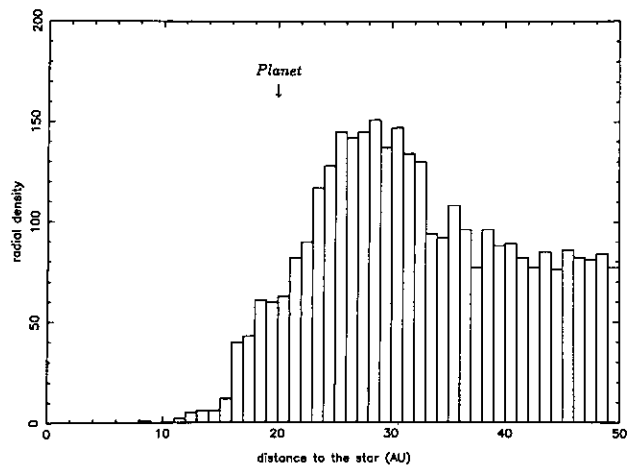

FIG. 9. Steady state radial density of particles corresponding to the simulation of the model C9 (see Table I). The total duration of the run is 10,000 $T_{pl} \sim 0.7 \times 10^6$ years. The half maximum density is near the planet orbit (20 AU). See the text for details.

5.5. *Varying the Parameters*

The mass of the planet is the most important parameter in the trapping mechanism. Figure 8 illustrates that there is a critical planetary mass of $\sim 10^{-5}\ M_\star$, above which trapping becomes significant. This corresponds to about one third of Uranus's mass, or five times Earth's mass. With this mass, however, the confining mechanism is visible for some particles, but it is not strong enough to stop the fall of the disk onto the star. With a mass of $10^{-4}\ M_\star$ (about one half of Saturn's mass), a planet is able to trap *all* the particles in one resonance or another. In this case, they remain locked at the same semimajor axis for more than 10,000 planetary revolutions ($\sim 0.7 \times 10^6$ years).

It appears difficult to derive an analytical expression for the probability of capture into a resonance, for a given planet mass. This problem is addressed in Paper 2 (see also the review by Malhotra 1993), where it is shown that the capture depends critically on the eccentricity e and the resonant angle Ψ_L just at the entrance into the resonance. In an (e, Ψ_L) diagram, the regions of capture exhibit complex patterns, with no obvious symmetries or clear structures. In any case, this study confirms that for masses larger than $\sim 10^{-5}\ M_\star$, most of the particles with an initial eccentricity smaller than a few percent are trapped into a first order resonance (see Figs. 7, 8, and 9 of Paper 2).

The particle size, or more exactly, β, is also an important parameter. We have run models with β between 0.1 and 0.3, corresponding to ~2.7 to 8 μm particle radii, in the geometrical approximation (Eq. (7)). In the range 0.1 to 0.3, changing β has two effects:

First, the resonance locations are shifted inward as β increases (Eq. (16)). Note that for small particles, the number of exterior resonance radii which lie *outside* the planetary orbit decreases. For instance, there are 18 first order resonances outside the planetary orbit for $\beta = 0.1$ and only 5 of them for $\beta = 0.3$. Note also that a swarm of particles with different sizes have mixed resonance locations. The 1 : 2 resonance varies from 32 AU for $\beta = 0$ to 28 AU for $\beta = 0.3$.

Second, the value of the dissipation coefficient α, and thus, the time scale of orbital decay, changes in correspondence with changes in β. The smaller particles evolve faster. For particles evolving with gas drag, the probability of trapping is modified by the drag coefficient (Kary *et al.* 1993). The value of β does not affect the probability of trapping in our study. We do not see any significant difference in the number of trapped particles when β varies in the range 0.1–0.3. However, note that varying β changes two parameters at the same time which can affect the trapping probability in opposite senses, that is, the resonance location *and* the drag coefficient.

5.6. *Steady State Dust Distribution*

Inner clearing zone. We present in Fig. 9, as an example, the steady state radial distribution of dust, with a planet of mass $10^{-4}\ M_\star$, and with $\beta = 0.3$ (run C9). In this simulation, several "images" of the system have been superimposed, which is equivalent to reintroducing particles with identical initial conditions as the previous particles fall toward the star.

Due to the dispersion of eccentricities, the inner edge is not sharply defined, but we see nevertheless that the disk is strongly depleted when passing from ~25 to 10 AU. The clearing of the inner zone is *not* due to a trace of the initial conditions, but actually proceeds from two mechanisms: (i) particles ejected outside repopulate the outer regions of the disk; (ii) particles falling onto the star have large orbital eccentricities, and thus also large dissipation coefficients (Eq. (4)), which explains their rapid fall. This stems from the fact that the PR drag time scale, $a/\dot{a}$, is proportional to $(1 - e^2)^{3/2}/\alpha$ (Eq. (2)). Since $\alpha \propto 1/r^2$ (Eq. (4)), the value of α averaged over one orbit is proportional to $1 - e^2$. Consequently, $a/\dot{a}$ is proportional to $(1 - e^2)^{5/2}$. For instance, a particle with eccentricity ~0.5 decays twice as fast as a particle in a circular orbit.

Depleted zone associated to the planet location. The protection mechanism is such that the particles are at apocenter when they have a conjunction with the planet. The resonances with different q yield wavy patterns with different azimuthal symmetry numbers, which average out any azimuthal structures, *except* at conjunction. Hence, a depletion zone is expected near the planetary position (see, for instance, Fig. 5b).

Arc-like structures. If the planetary orbit is eccentric, the corotation resonances generate arc-like structures

with corotate with the particles, *not* with the planet, in contrast to the depletion zone decribed above. Note that these conspiscuous structures require only a moderate orbital eccentricity of the planet (10^{-2} in the example of Fig. 5). Considering the eccentricities of the planets in the Solar System, such structures should be expected in many circumstellar disks with embedded planets.

6. DISCUSSION

We have investigated a process in which a planet can induce large scale structures in a circumstellar disk composed of $\sim 1-20-\mu$m-sized particles. In the case of the β Pictoris disk, we have placed the planet at 20 AU from the star, in order to match the observations of an inner clearing zone. The main results that we have obtained are the following:

- There exists a critical planetary mass of $\sim 10^{-5}\, M_\star$, i.e., about 5 Earth masses, or $\frac{1}{3}$ Uranian masses, above which trapping in mean motion resonances is very efficient, in both the 2D and 3D cases.
- We have *not* observed *permanent* trappings into the resonances. However, the trapping time scale is comparable to the PR drag decay time scale, resulting in an accumulation of particles just outside the planet orbit.
- Once they escape the resonances, the particles rapidly decay onto the star, due to their enhanced eccentricities at that time.
- A moderate (10^{-2}) planetary orbital eccentricity can create large scale azimuthal (arclike) asymmetries in the disk.
- The protection mechanism associated to the resonances also creates a void region just outside the planet, and corotating with it.

Radial and azimuthal structures caused by a planet with mass $10^{-4}\, M_\star$ are summarized in Figs. 5b and 9.

Several questions remain open, however. From a purely dynamical point of view, the problem of the escape from a resonance, near the equilibrium eccentricity e_{eq}, is not fully understood. Analytical approaches which can handle large eccentricities properly are now required. Also, numerical integrations which accurately describe (singular) close encounters with the planet are needed. In particular, one can ask whether particles are preferentially ejected outside or inside the planet orbit. The distribution of eccentricities for these ejected particles should also be clarified.

Gas drag and high velocity collisions should also be considered at some point. The present observations make it difficult to estimate the neutral gas density in circumstellar disks, but some numerical investigations would be worthwhile. In view of the universality of resonance dissipation effects, one should expect that gas drag will also result in resonance trapping and arclike structures. Of course, this requires some more specific studies.

Finally, this work should be connected to the detection of infalling material, deduced from red-shifted absorption lines observed along the line of sight. Models indicate that this material could be released from evaporating comets on highly eccentric orbits (Beust *et al.* 1990, 1991, Beust and Tagger 1993). It is now important to better assess the perturbing effects of a planet, or several planets, on a swarm of comets.

ACKNOWLEDGMENTS

We thank R. Malhotra for several constructive remarks, and D. R. Davis for a very detailed review of this paper. The calculations were carried out on the Connection Machine CM-2 at INRIA, Sophia Antipolis. This research was supported in part by the National Science Foundation under Grant N0 PHY89-04035, and by the Programme National de Planétologie. F. Roques thanks the Institute of Theoretical Physics at Santa Barbara, where part of this work was done, for its hospitality during the research program *Planet Formation* organized by J. J. Lissauer (September–December 1992).

REFERENCES

ARTYMOWICZ, P., C. BURROWS, AND F. PARESCE 1989. The structure of the Beta Pictoris circumstellar disk from combined *Iras* and coronographic observations. *Astrophys. J.* **337,** 494–513.

AUMANN, H. 1988. Spectral class distribution of circumstellar material in the main-sequence stars. *Astron. J.* **96,** 1415–1419.

BACKMAN, D. E. AND F. C. GILLETT 1987. Exploring the infrared: IRAS observations of the main sequence. In *Cool Stars, Stellar Systems and the Sun* (J. L. Linsky and R. E. Stencel, Eds.), pp. 340–350. Springer-Verlag, Berlin/Heidelberg.

BACKMAN, D. E., F. C. GILLETT, AND F. C. WITTERBORN 1992. Infrared observations and thermal models of the β Pictoris disk. *Astrophys. J.* **385,** 670–679.

BASRI, G., AND C. BERTOUT 1993. T Tauri stars and their accretion disks. In *Protostars and Planets III* (Levy, E. H., and J. I. Lunine Eds.), pp. 543–566. Univ. Arizona Press, Tucson.

BEAUGÉ, C. 1993. Asymmetric librations in exterior resonances. Submitted for publication.

BEAUGÉ, C., AND S. FERRAZ-MELLO 1993. Resonance trapping in the primordial solar nebula: The case of a Stokes drag dissipation. *Icarus* **103,** 301–318.

BECKWITH, S. V. W., A. I. SARGENT, R. S. CHINI, AND R. GÜNSTEN 1990. A survey for circumstellar disks around young stars. *Astrophys. J.* **99,** 924–945.

BECKWITH, S. V. W., AND A. I. SARGENT 1993. The occurrence and properties of disks around young stars. In *Protostars and Planets III* (E. H. Levy, and J. I. Lunine, Eds.), pp. 521–541. Univ. of Arizona Press, Tucson.

BEUST, H., A. M. LAGRANGE-HENRI, A. VIDAL-MADJAR, AND R. FERLET 1990. The β-Pictoris circumstellar disk. X. Numerical simulations of infalling evaporating bodies, *Astron. Astrophys.* **236,** 202–216.

BEUST, H. 1991. "Dynamique interne du disque protoplanétaire autour de l'étoile β-Pictoris." *Thèse de Doctorat,* Université de Paris 7.

BEUST, H., A. VIDAL-MADJAR, R. FERLET, AND A. M. LAGRANGE-HENRI 1991. The β-Pictoris circumstellar disk. XII. Planetary perturbations in the disk and star-grazing bodies. *Astron. Astrophys.* **247,** 505–515.

BEUST, H., AND M. TAGGER 1993. A hydrodynamical model for infalling

evaporating bodies in the β Pictoris circumstellar disk. *Icarus* **106,** 42–58.

BOGGESS, A., F. C. BRUHWEILER, C. A. GRADY, D. EBBETS, Y. KONDO, L. M. TRAFTON, J. BRANDT, AND S. R. HEAP 1991. First results from the Goddard high-resolution spectrograph: Resolved velocity and density structure in the β Pictoris circumstellar gas. *Astrophys. J.* **377,** L49–L52.

BURNS, J. A., P. L. LAMY, AND S. SOTER 1979. Radiation forces on small particles in the solar system. *Icarus* **40,** 1–48.

CHINI, R., E. KRÜGEL, AND E. KREYSA 1990. Large dust particles around main sequence stars. *Astron. Astrophys.* **277,** L5–L8.

CHINI, R., E. KRÜGEL, B. SHUSTOV, A. TUTUKOV, AND E. KREYSA 1991. Dust disks around Vega-type stars. *Astron. Astrophys.* **252,** 220–228.

FERLUGA, S. 1990. Epsilon Aurigae. I. Multi-ring structure of the eclipsing body. *Astron. Astrophys.* **238,** 270–278.

GOLDREICH, P., AND S. TREMAINE 1982. The dynamics of planetary rings. *Ann. Rev. Astron. Astrophys.* **20,** 249–283.

GOLDREICH, P., S. TREMAINE, AND N. BORDERIES 1986. Towards a theory for Neptune's arc rings. *Astron. J.* **92,** 490–494.

GOLIMOWSKI, D. A., S. T. DURRANCE, AND M. CLAMPIN 1993. Coronographic imaging of the Beta Pictoris circumstellar disk: Evidence of changing disk structure within 100 A. U. submitted for publication.

GONCZI, R., CH. FROESCHLÉ, AND CL. FROESCHLÉ 1982. Poynting–Robertson drag and orbital resonance. *Icarus* **51,** 633–654.

GRADY, C. A., AND J. M. S. SILVIS 1993. The circumstellar gas surrounding 51 Ophiuchus: A candidate proto-planetary system similar to β-Pictoris. *Astrophys. J.* **402,** L61–L64.

GREENBERG, R. 1978. Orbital resonance in a dissipative medium. *Icarus* **33,** 62–73.

GREENBERG, R. 1983. The role of dissipation in shepherding of ring particles. *Icarus* **53,** 207–218.

HOBBS, L. M. 1986. Observations of gaseous circumstellar disks, III. *Astrophys. J.* **308,** 854–858.

JACKSON, A. A., AND H. A. ZOOK 1989. A solar system dust ring with the Earth as its shepherd. *Nature* **337,** 629–631.

JACKSON, A. A., AND H. A. ZOOK 1992. Orbital evolution of dust particles from comets and asteroids. *Icarus* **97,** 70–84.

KARY, D. M., J. LISSAUER, AND Y. GREENZWEIG 1993. Nebular gas drag and planetary accretion. *Icarus* **106,** 288–307.

LAGAGE, P. O., AND E. PANTIN 1993. Sub-arcsec 10 μm imaging of β Pictoris and other stars disk candidates. In *Infrared Astronomy with Arrays: The Next Generation* (I. McLean, Ed.). Kluwer Academic, Dordrecht, in press.

LANZEROTTI, L. J., W. L. BROWN, J. M. POATE, AND W. M. AUGUSTNIAK 1978. Low energy cosmic ray erosion of ice grains in interplanetary and interstellar media, *Nature* **272,** 431–433.

LAZZARO, D., B. SICARDY, F. ROQUES, AND R. GREENBERG 1994. Is there a planet around β Pictoris? Perturbations of a planet on a circumstellar dust disk. 2. Analytical model. *Icarus* **108,** 59–80.

LECAVELIER DES ETANGS, A., G. PERRIN, R. FERLET, A. VIDAL-MADJAR, F. COLAS, C. BUIL, F. SÈVRE, J.-E. ARLOT, H. BEUST, A.-M., LAGRANGE-HENRI, J. LECACHEUX, M. DELEUIL, AND C. GRY 1993. Observations of the central part of the β-Pictoris disk with an anti-blooming CCD. *Astron. Astrophys.* **274,** 877–882.

LEINERT, C., AND E. GRÜN 1990. Interplanetary dust. In *Physics of the Inner Solar Heliosphere I* (R. Schwenn and E. Marsch, Eds.), pp. 207–275. Springer–Verlag, Berlin/Heidelberg.

LISSAUER, J. J. 1987. Timescales for planetary accretion and the structure of the protoplanetary disk. *Icarus* **69,** 249–265.

LISSAUER, J. J. 1993. Planet formation. *Ann. Rev. Astron. Astrophys.* **31,** 129–174.

MALHOTRA, R. 1993. Orbital resonances in the Solar Nebula: Strengths and weaknesses. *Icarus* **106,** 264–273.

MEYER-VERNET, N., AND B. SICARDY 1987. On the physics of resonant disk-satellite interaction. *Icarus* **69,** 157–175.

NORMAN, C. A., AND F. PARESCE 1989. Circumstellar material around nearby stars: Clues to the formation of planetary systems. In *The Formation and Evolution of Planetary Systems* (H. Weaver and L. Danby, Eds.), pp. 151–169. Cambridge Univ. Press, London/New York.

PARESCE, F., AND C. BURROWS 1987. Broad-band imaging of the Beta Pictoris circumstellar disk. *Astrophys. J.* **319,** L23–L25.

PARESCE, F. 1991. On the evolutionnary status of β Pictoris. *Astron. Astrophys.* **247,** L25–L27.

PARESCE, F. 1992. The search for extra-solar planetary systems. *Adv. Space Res.* **12,** 157–167.

PATTERSON, C. W. 1987. Resonance capture and the evolution of the planets. *Icarus* **70,** 319–333.

PORCO, C. C. 1991. An explanation for Neptune's ring arcs. *Science* **253,** 995–1001.

ROQUES, F., B. SICARDY, H. SCHOLL, AND B. A. SMITH 1990. Confinement of dust by a planet in circumstellar disk. *Bull. Am. Astron. Soc.* **22,** 1079.

SCHOLL, H., F. ROQUES, AND B. SICARDY 1993. Resonance trapping of circumstellar dust particles by an alleged planet. *Celestial. Mech.* **56,** 381–393.

SICARDY, B. 1991. Numerical exploration of planetary arcs dynamics, *Icarus* **89,** 197–219.

SICARDY, B., C. BEAUGÉ, S. FERRAZ-MELLO, D. LAZZARO, AND F. ROQUES 1993. Capture of grains into resonances through Poynting–Robertson drag. *Celestial Mech.* **57,** 373–390.

SMITH, B. A., AND R. J. TERRILE 1984. A circumstellar disk around β-Pictoris. *Science* **226,** 1421–1424.

SMITH, B. A., AND R. J. TERRILE 1987. The Beta-Pictoris disk: Recent optical observations. *Bull. Am. Astron. Soc.* **19,** 829.

STERN, S. A., M. FESTOU, AND D. A. WEINTRAUB 1993. α Piscis Austrini. *IAU Circular 5732.*

TELESCO, C. M., E. E. BECKLIN, R. D. WOLSRENCROFT, AND R. DECHER 1988. Resolution of the circumstellar disk of β Pictoris at 10 and 20 μm. *Nature* **335,** 51–53.

VIDAL-MADJAR, A., A. LECAVELIER DES ETANG-LEVALLOIS, G. PERRIN, R. FERLET, F. SÈVRE, F. COLAS, J.-E., ARLOT, C. BUIL, H. BEUST, A. M. LAGRANGE-HENRI, AND J. LECACHEUX 1992. Observations of the central part of the β-Pictoris disk with an anti-blooming CCD. *The Messenger* **69,** 45–48.

WEIDENSCHILLING, S. J. 1977. Aerodynamics of solid bodies in the solar system. *Icarus* **180,** 57–70.

WEIDENSCHILLING, S. J., AND D. R. DAVIS 1985. Orbital resonances in the Solar Nebula: Implications for planetary accretion, *Icarus* **62,** 16–29.

WEIDENSCHILLING, S. J., AND A. A. JACKSON 1993. Orbital resonances and Poynting–Robertson drag. *Icarus* **104,** 244–254.

WHITMIRE, D. P., J. J. MATESE, AND L. J. TOMLEY 1989. A brown dwarf companion as an explanation of the asymmetry in the Beta Pictoris disk. *Astron. Astrophys.* **203,** L13–L15.

ZUCKERMAN, B., AND E. E. BECKLIN 1993. Submillimeter studies of main-sequence stars. *Astrophys. J.* **414,** 793–802.